Advances in Nano Research, *Vol. 16, No.6 (2024) 549-564*
https://doi.org/10.12989/anr.2024.16.6.549

An accurate analytical exploration for dynamic response of thermo-electric CNTRC beams under driving harmonic and constant loads resting on Pasternak foundation

Mohammadreza Eghbali[1] and Seyed Amirhosein Hosseini*[2]

[1]*Department of Mechanical Engineering, University of Zanjan, Zanjan, Iran*
[2]*Department of Industrial, Mechanical and Aerospace Engineering, Buein Zahra Technical University, Qazvin, Iran*

(*Received December 27, 2021, Revised May 1, 2022, Accepted April 26, 2024*)

Abstract. This paper aims to analyze the dynamic response of thermoelectric carbon nanotube-reinforced composite (CNTRC) beams under moving harmonic load resting on Pasternak elastic foundation. The governing equations of thermoelectric CNTRC beam are obtained based on the Karama shear deformation beam theory. The beams are resting on the Pasternak foundation. Previous articles have not performed the moving load mode with the analytical method. The exact solution for the transverse and axial dynamic response is presented using the Laplace transform. A comparison of previous studies has been published, where a good agreement is observed. Finally, some examples were used to analyze, such as excitation frequency, voltage, temperature, spring constant factors, the volume fraction of Carbon nanotubes (CNTs), the velocity of a moving harmonic load, and their influence on axial and transverse dynamic and maximum deflections. The advantages of the proposed method compared to other numerical methods are zero reduction of the error percentage that exists in numerical methods.

Keywords: analytical solution; CNTRC beams; driving harmonic and constant loads; Laplace transform; Pasternak foundation; thermoelectric effects

1. Introduction

The discovery of multi-walled tubes in 1991 has caused extensive research activities in the sciences to be devoted to discussing carbon nanotubes and their applications. The main reason for this is their expected structural evolution, small size, low density, high hardness, high strength, and excellent electrical properties. So far, extraordinary qualities have been obtained from this material, including mechanical resistance, low weight, thermal conductivity, different electronic behavior, and its most external tensile strength (Kaiser *et al*. 2011, Ebrahimi *et al*. 2015, Hosseini and Rahmani 2016, Hayati *et al*. 2017, Ghadiri *et al*. 2018, Hamidi *et al*. 2018, 2020, Alizade Hamidi *et al*. 2019, 2021, Behrouz *et al*. 2019, Bensattalah *et al*. 2019, 2020, Alizadeh Boulal *et al*. 2020, Gafour *et al*. 2020, Hosseini *et al*. 2020, Khosravi and Hosseini 2020, Khosravi 2020a, b, Ghadiri Rad *et al*. 2021).

According to research conducted by the University of California, people who suffer from osteoporosis and bone fractures, their problem is solved with the help of carbon nanotubes. The strength, flexibility, and lightweight carbon nanotubes allow researchers to use them as splints or scaffolds to regenerate broken bones. The researchers' findings have improved the flexibility and strength of artificial bones and created new types of bone grafts to treat bone diseases. Artificial bones are made from various materials, such as polymers or peptide filaments, but the problem is that they are not very strong and may not be accepted by the body. Single-walled carbon nanotubes are very strong materials. Because the bone is a natural composite composed of a mixture of organic and inorganic materials, nanotubes can be an excellent alternative to the organic part of the bone. Osteoporosis is a natural composite of collagen fibers and hydroxyapatite crystals based on the mineral calcium phosphate. In their experiments on mice, the scientists used this type of fluid, which contained the proteins, on open wounds and in a variety of tissues, including tissues such as the brain, kidneys, skin, and nerve fibers. In all of these cases, they could immediately control the bleeding in the damaged tissue and blood vessels (Nielsen 1974, Zhang and Li 2009, Tounsi *et al*. 2013, Mohammadjani and Shariyat 2020, Tayeb *et al*. 2020, Zerrouki *et al*. 2020, Shariyat and Abedi 2022).

Şimşek and Reddy (2013) investigated the vibrations of a functional calibrated microbeam using high-order theory using nonlocal theory. Shen and Xiang (2013) studied the carbon nanotubes nonlinearly in a thermal environment. Wattanasakulpong *et al*. studied the buckling, bending, and vibrations of carbon nanotubes using an analytical solution (Wattanasakulpong and Ungbhakorn 2013). Mantari *et al* (2014) dealt with a variety of higher-order theories for composite sheets. Hosseini and Rahmani (2017) investigated the transverse and axial displacement of a functionally graded nanobeam under moving load. Bensattalah *et al*. (2019) analyzed Timoshenko nanobeam reinforced with three-walled carbon tubes. The equations were derived

*Corresponding author, Professor,
E-mail: hosseini@bzte.ac.ir

Copyright © 2024 Techno-Press, Ltd.

ISSN: 2287-237X (Print), 2287-2388 (Online)

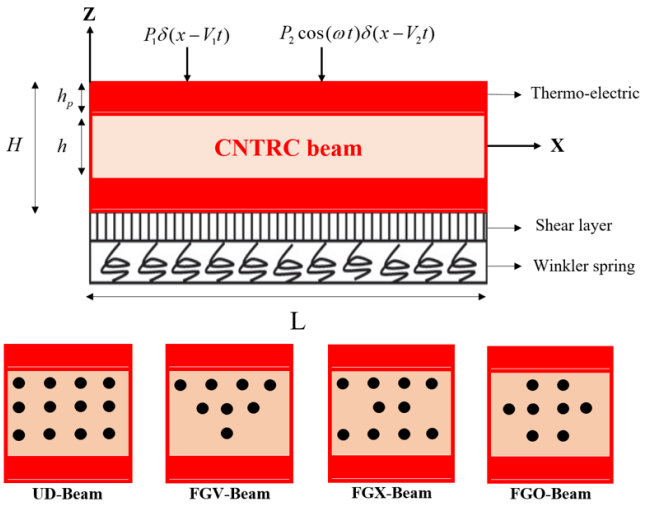

Fig. 1 Geometry of a CNTRC thermoelectric beam on Pasternak foundation

using nonlocal elasticity theory and zigzag theory. Bensattalah *et al*. (2016) analyzed the free vibrations of Euler-Bernoulli and Timoshenko nanobeam in a temperature environment. Equations were extracted using the theory of nonlocal elasticity. Material properties are temperature-dependent. Zerrouki *et al*. (2020) critical buckling analyses of nonlinear FG-CNT reinforced nano-composite beam.

Here are the latest works. Abdelrahman *et al*. (2021) studied the dynamic analysis of carbon nanobeam reinforced on elastic foundation. Alazwari *et al*. (2021) studied the static analysis of multilayer carbon nanotubes. Babaei (2022) examined Free vibration and snap-through instability of FG-CNTRC shallow arches supported on nonlinear elastic foundation. Babaei *et al*. (2021a, b) studied the vibrations of carbon nanotubes in different thermal environments and different boundary conditions. Civalek *et al*. studied the free and forced vibrations of carbon nanotubes with zigzag theory (Chalak *et al*. 2021, Civalek 2021a, b). Ebrahimi *et al*. studied the free and torsional vibrations of sandwich beams in thermal, magnetic and electric environments with the face layer of carbon nanotubes and graphene oxide (Ebrahimi *et al*. 2021a, b, c).

Eghbali *et al*. (2021) studied the free vibration of axially functionally graded nanobeam with an attached mass based on nonlocal strain gradient theory via the new ADM numerical method. Garg *et al*. (2022) examined the free vibrations of a carbon-reinforced sandwich beam with a softcore. Heidari *et al*. (2021) studied the free vibrations of a carbon cylinder reinforced with a nanotube.

Madenci examined free vibration analysis of carbon nanotube RC nanobeams with variational approaches (Madenci 2021). Serajzadeh *et al*. studied two-dimensional low-velocity impact analysis of curved sandwich beams with FG-CNTRC face sheets and porous core (Serajzadeh and Malekzadeh 2021). Van Quyen *et al*. (2021) studied nonlinear forced vibration of the cylindrical sandwich panel with negative Poisson's ratio auxetic honeycombs core and CNTRC face sheets. Xu *et al*. (2021a, b) analyzed the vibrations of FG carbon nanotubes in a thermal environment with general boundary conditions. Zheng *et al*. (2021) studied forced vibration characteristics of embedded graphene oxide powder reinforced metal foam nano-composite plate in a thermal.

This paper aimed to analyze the axial and transverse dynamic response of CNTRC beams under moving harmonic and constant load. The governing equations of the CNTRC beam are obtained based on the Karama shear deformation beam theory and Laplace transform to solve the derived differential equations. It should be noted that an exact solution for both transverse and axial responses is obtained due to this effort. Through parametric study, valuable results have been concluded related to the effect of essential parameters such as excitation frequency, voltage, temperature, spring constant factors, the volume fraction of CNTs, and load velocity on the dynamic response of the thermoelectric CNTRC beams in axial and transverse modes. The presented results in this study are validated by obtaining good agreement, which compares with available results in the literature.

2. Formulation of the problem

2.1 CNTRC beams

A CNTRC thermoelectric beam is considered from a single-walled carbon nanotube (SWCNT) and anisotropic polymer matrix. The beam, having length (L) and height (h) with surface-bonded thermoelectric layers with a thickness h_p, is placed on the Pasternak elastic foundation, including a shear layer and Winkler spring. In this study, the beams are assumed to have four different reinforcement patterns over the cross-sections, shown in Fig. 1.

$$\begin{aligned} E_{11} &= \eta_1 V_{CN} E_{11}^{CN} + V_k E^k \\ \frac{\eta_2}{E_{22}} &= \frac{V_{CN}}{E_{22}^{CN}} + \frac{V_k}{E^k} \\ \frac{\eta_3}{G_{12}} &= \frac{V_{CN}}{G_{12}^{CN}} + \frac{V_k}{G^k} \end{aligned} \tag{1}$$

where G_{12}^{CN}, E_{22}^{CN} and E_{11}^{CN} are defined as the shear modulus and Young's modulus, respectively, and E^k, G^k as the properties of the polymer matrix. Also, V_{CN} and V_k are the volume fraction for the carbon nanotube and polymer matrix, respectively, with the relation of $V_{CN} + V_k = 1$. To consider the size dependent material properties, the CNT efficiency parameters, $\eta_i = (i = 1,2,3)$, are introduced. They can be determined from the matching of the elastic modulus of estimated by MD simulation with the numerical results estimated by the mixed rule. By using the same rule, Poisson's ratio (υ) and mass density (ρ) of the CNTRC beams are written as

$$\upsilon_h = V_{CN}\upsilon_{CN} + V_k\upsilon^k \tag{2}$$

$$\rho_h = V_{CN}\rho_{CN} + V_k\rho^k \tag{3}$$

The thermal expansion coefficient can be expressed as:

$$\alpha_h = V_{CN}\alpha_{11}^{CN} + V_k\alpha^k \tag{4}$$

The expressions of the effective Young's modulus and shear modulus of CNTRC beams are as follows (Shen and Xiang 2013)

L	Length	V_{CN}^{*}	Volume fraction
h	Height	O_{CN}	Mass fraction
h_p	Thermoelectric layers thickness	η_i	CNT Efficiency parameters
G	Shear modulus	u_0	Axial displacement
E	Young's modulus	w_0	Transverse displacement
ρ	Mass density	$\Psi(z)$	Shape function
α	Thermal expansion coefficient	ϕ_0	Total bending rotation
υ	Poisson's ratio	t	Time
σ_{xx}	Normal stress	k_s	Shearing layer spring constants
σ_{xz}	Shear stress	$\beta_w,\ \beta_s$	Spring constant factors
σ_{xx}^{T}	Thermoelectric stress	A_{110}	Extension stiffness
C_{11}	Reduced elastic constant	f	Transverse load
k_w	Winkler layer spring constants	V_1, V_2	Velocity of moving load
N_{x0}	Axially compressive force	U	Virtual strain energy
N_x, M_x, P_x, Q_x	Stress resultants	V	Virtual work
$\bar{\omega}$	Dimensionless natural frequencies	K	Virtual kinetic energy
ω	Excitation frequency	I	Mass moments of inertia

where υ_{CN}, υ^k, ρ_{CN}, ρ^k and α^k are the Poisson's ratios, densities, and thermal expansion coefficients of the CNT and polymer matrix, respectively. The continuous mathematical functions are used to describe the distribution of the components of the following elements:

$$\begin{aligned}&\text{UD-Beam:} V_{CN} = V_{CN}^{*}\\ &\text{V-Beam:} V_{CN} = (1+\frac{2z}{h})V_{CN}^{*}\\ &\text{O-Beam:} V_{CN} = 2(1-\frac{2|z|}{h})V_{CN}^{*}\\ &\text{X-Beam:} V_{CN} = 2(\frac{2|z|}{h})V_{CN}^{*}\end{aligned} \tag{5}$$

where V_{CN}^{*} is the given volume fraction of CNTs, which is derived from the following equation:

$$V_{CN}^{*} = \frac{O_{CN}}{O_{CN} + (\frac{\rho_{CN}}{\rho_k}) - (\frac{\rho_{CN}}{\rho_k})O_{CN}} \tag{6}$$

where O_{CN} is the mass fraction of CNT. From Eq. (5), It can be defined that the beams O -, X - and V - are some form of functional calibrated beams where their constituent materials continuously change in their thickness, at the same time, the V-Beam has uniformly distributed carbon nanotube reinforcement. In this work, the CNT efficiency parameters (η_i) associated with the given volume fraction (V_{CN}^{*}) are: $\eta_1 = 1.2833$ and $\eta_2 = \eta_3 = 1.0556$for $V_{CN}^{*} = 0.12$, $\eta_1 = 1.3414$ and $\eta_2 = \eta_3 = 1.7101$ for $V_{CN}^{*} = 0.17$, $\eta_1 = 1.3238$ and $\eta_2 = \eta_3 = 1.7380$ for $V_{CN}^{*} = 0.28$ (Shen and Xiang 2013).

2.2 Equations of motion

The shear deformation beam theory, the axial and transverse displacement field can be expressed as follows:

$$\begin{aligned}u(x,z,t) &= u_0 - z\frac{\partial w_0(x,t)}{\partial x} + \Psi(z)f_0(x,t)\\ w(x,z,t) &= w_0(x,t)\end{aligned} \tag{7}$$

where u_0 and w_0 are the axial and transverse displacement, respectively $\Psi(z)$ shape function. f_0 and $\Psi(z)$, defined as the transverse shear strain, can be expressed as (Mantari *et al*. 2014)

$$\begin{aligned}f_0(x,t) &= \frac{\partial w_0(x,t)}{\partial x} - \phi_0(x,t)\\ \Psi(z) &= ze^{[-2(\frac{z}{h})^2]}\end{aligned} \tag{8}$$

where ϕ_0 is the total bending rotation of the cross-section, and t is time. The expression of normal and shear strain components associated with the displacement field in Eq. (7) follows.

$$\varepsilon_{xx} = \frac{\partial u_0}{\partial x} - z\frac{\partial^2 w_0}{\partial x^2} + \Psi(z)(\frac{\partial^2 w_0}{\partial x^2} - \frac{\partial \phi_0}{\partial x}) \tag{9}$$

$$\gamma_{xz} = \frac{\partial \Psi(z)}{\partial z}(\frac{\partial w_0}{\partial x} - \phi_0) \tag{10}$$

The normal, shear, and thermoelectric stress, respectively σ_{xx}, σ_{xz} and σ_{xx}^{T} including thermal effect, is given by the linear elastic constitutive law as:

$$\sigma_{xx} = E_{11}(z,t)\left\{\frac{\partial u_0}{\partial x} - z\frac{\partial^2 w_0}{\partial x^2} + \Psi(z)(\frac{\partial^2 w_0}{\partial x^2} - \frac{\partial \phi_0}{\partial x})\right\} \tag{11}$$

$$\sigma_{xx}^{T} = C_{11}(z,t)\left\{\frac{\partial u_0}{\partial x} - z\frac{\partial^2 w_0}{\partial x^2} + \Psi(z)(\frac{\partial^2 w_0}{\partial x^2} - \frac{\partial \phi_0}{\partial x})\right\} \tag{12}$$

$$\begin{aligned}\sigma_{xz} &= \frac{E_{11}(z)}{1-{\upsilon_h}^2(z)}\gamma_{xz},\\ Q_{55}(z) &= G_{12}(z),\\ Q_{55}^{T}(z) &= \frac{C_{11}(z)}{2(1-\upsilon_T(z))}\end{aligned} \tag{13}$$

where in Eq. (12):

$$E_z = \frac{\text{Voltage}}{h_p} \tag{14}$$

The thermoelectric material properties are temperature independent, and C_{11}, α_p denotes the reduced elastic constant and thermal expansion coefficient, respectively. The reduced elastic modulus E, thermal expansion coefficient α, and density ρ are piecewise functions to variable z as:

$$(E,\alpha,\rho,\upsilon) = \left\{\begin{matrix}\begin{pmatrix}C_{11}\\ E_{11}\\ C_{11}\end{pmatrix},\begin{pmatrix}\alpha_T\\ \alpha_h\\ \alpha_T\end{pmatrix},\begin{pmatrix}\rho_T\\ \rho_h\\ \rho_T\end{pmatrix},\begin{pmatrix}\upsilon_T\\ \upsilon_h\\ \upsilon_T\end{pmatrix} & -\frac{H}{2} \le z \prec -\frac{h}{2}\\ & -\frac{h}{2} \le z \prec \frac{h}{2}\\ & \frac{h}{2} \le z \prec \frac{H}{2}\end{matrix}\right\} \tag{15}$$

2.3 Hamilton principle

To obtain the equations of motion, Hamilton's principle is employed as follows:

$$\int_{t_1}^{t_2}(\delta V-\delta K+\delta U)dt=0,\delta U=\delta U_h+\delta U_g \quad (16)$$

where δV do external forces do the virtual work, δK is the virtual kinetic energy andδU is the virtual variation of the total strain energy. The initial and final time is defined as t_1 and t_2, respectively. Each of these quantities in Eq. (16) is derived next.

Strain energy $\delta U=\delta U_h+\delta U_g$ is composed of the virtual strain energy of the beam δU_h and the virtual potential energy of the elastic foundation δU_g. The virtual strain energy of the beam:

$$\begin{aligned}\delta U_h=&\int_A\int_{-\frac{H}{2}}^{\frac{H}{2}}(\sigma_{xx}\,\delta\varepsilon_{xx}+\sigma_{xz}\delta\gamma_{xz})dxdydz=\\&\int_A(N_x\frac{d\delta u_0}{dx}-M_x\frac{d^2\delta w_0}{dx^2}+P_x(\frac{d^2\delta w_0}{dx^2}-\frac{d\delta\phi_0}{dx})\\&+Q_x(\frac{d\delta w_0}{dx}-\delta\phi_0))\,dA\end{aligned} \quad (17)$$

$$\begin{aligned}\delta U_g=&\int_0^L(k_w w_0\delta w_0-k_s\frac{dw_0}{dx}\frac{d\delta w_0}{dx})\,dx\\k_w=&\frac{\beta_w A_{110}}{L^2},k_s=\beta_s A_{110}\end{aligned} \quad (18)$$

In Eq. (17), k_w and k_s are the Winkler and shearing layer spring constants. β_w and β_s are the corresponding spring constant factors. It is also defined that A_{110} is the extension stiffness or the value of A_{11} of a homogeneous beam made of the pure matrix material.

The virtual work done (δV) can be expressed as:

$$\begin{aligned}\delta V=&-\int_0^L\left(f\delta w_0+N_{x0}\frac{dw_0}{dx}\frac{d\delta w_0}{dx}\right)dx\\N_{x0}=&N^T+N^P,\\f=&P_1\delta(x-V_1t)+P_2\,cos(\omega t)\delta(x-V_2t)\end{aligned} \quad (19)$$

where the transverse load (f), ω is excitation frequency, V_1 and V_2 velocity of moving constant and harmonic load $\delta(.)$is Dirac delta function, and axially compressive force (N_{x0})

For the dynamic case, the virtual kinetic energy (δK) is required for the equations of motion, which takes the form:

$$\begin{aligned}\delta K=&\int_0^L\rho(z)\,[\dot u\delta\dot u+\dot w\delta\dot w]dAdx=\\&\int_0^L\begin{Bmatrix}I_0(\dot u_0\delta\dot u_0+\dot w_0\delta\dot w_0)-I_1(\frac{d\dot w_0}{dx}\delta\dot u_0+\dot u_0\frac{d\delta\dot w_0}{dx})\\+I_2\left(\frac{d\dot w_0}{dx}\frac{d\delta\dot w_0}{dx}\right)\\+I_3(\frac{d\dot w_0}{dx}\delta\dot u_0-\dot\phi_0\delta\dot u_0+\dot u_0\frac{d\delta\dot w_0}{dx}-\dot u_0\delta\dot\phi_0)\\+I_4(\dot\phi_0\frac{d\delta\dot w_0}{dx}-2\frac{d\dot w_0}{dx}\frac{d\delta\dot w_0}{dx}+\frac{d\dot w_0}{dx}\delta\dot\phi_0)+\\I_5(\frac{d\dot w_0}{dx}\frac{d\delta\dot w_0}{dx}-\dot\phi_0\frac{d\delta\dot w_0}{dx}-\frac{d\dot w_0}{dx}\delta\dot\phi_0+\dot\phi_0\delta\dot\phi_0)\end{Bmatrix}dx\end{aligned} \quad (20)$$

The stress results are extracted as:

$$N_x=\int_{-\frac{h}{2}}^{\frac{h}{2}}\sigma_{xx}dz+\int_{\frac{h}{2}}^{\frac{h}{2}+h_P}\sigma_{xx}^T dz+\int_{-(\frac{h}{2}+h_P)}^{-\frac{h}{2}}\sigma_{xx}^T dz \quad (21)$$

$$M_x=\int_{-\frac{h}{2}}^{\frac{h}{2}}z\sigma_{xx}dz+\int_{\frac{h}{2}}^{\frac{h}{2}+h_P}z\sigma_{xx}^T dz+\int_{-(\frac{h}{2}+h_P)}^{-\frac{h}{2}}z\sigma_{xx}^T dz \quad (22)$$

$$\begin{aligned}P_x=&\int_{-\frac{h}{2}}^{\frac{h}{2}}\Psi(z)\sigma_{xx}dz+\int_{\frac{h}{2}}^{\frac{h}{2}+h_P}\Psi(z)\sigma_{xx}^T dz\\&+\int_{-(\frac{h}{2}+h_P)}^{-\frac{h}{2}}\Psi(z)\sigma_{xx}^T dz\end{aligned} \quad (23)$$

$$\begin{aligned}Q_x=&\int_{-\frac{h}{2}}^{\frac{h}{2}}\frac{d\Psi(z)}{dz}\sigma_{xz}dz+\int_{\frac{h}{2}}^{\frac{h}{2}+h_P}\frac{d\Psi(z)}{dz}\sigma_{xz}^T dz\\&+\int_{-(\frac{h}{2}+h_P)}^{-\frac{h}{2}}\frac{d\Psi(z)}{dz}\sigma_{xz}^T dz\end{aligned} \quad (24)$$

N_x, M_x, P_x, and Q_x are the stress resultants in the normal, bending moment, higher-order generalized, and sheer force. Where the superscripts "T" and "P" in Eq. (18) represent the thermal and electric loads, respectively, and N^T, M^T as well as N^P, M^P is defined as:

$$\begin{aligned}\begin{pmatrix}N^T M^T\\N^P M^P\end{pmatrix}=&\int_{-\frac{h}{2}}^{\frac{h}{2}}\begin{pmatrix}E_{11}\alpha\Delta T\\E_{11}d_{31}E_z\end{pmatrix}[1,z]dz\\+&\int_{\frac{h}{2}}^{\frac{h}{2}+h_P}\begin{pmatrix}C_{11}\alpha\Delta T\\C_{11}d_{31}E_z\end{pmatrix}[1,z]dz\\+&\int_{-(\frac{h}{2}+h_P)}^{-\frac{h}{2}}\begin{pmatrix}C_{11}\alpha\Delta T\\C_{11}d_{31}E_z\end{pmatrix}[1,z]dz\end{aligned} \quad (25)$$

where the superposed dot on a variable indicates time derivative and I_i *(i = 0,1,2...5)* are the mass moments of inertia defined as:

$$\begin{aligned}[I_0,I_1,I_2]=&\int_{-\frac{h}{2}}^{\frac{h}{2}}\rho_h[1,z,z^2]dz\\+&\int_{\frac{h}{2}}^{\frac{h}{2}+h_P}\rho_T[1,z,z^2]dz+\int_{-(\frac{h}{2}+h_P)}^{-\frac{h}{2}}\rho_T[1,z,z^2]dz\end{aligned} \quad (26)$$

$$\begin{aligned}[I_3,I_4]=&\int_{-\frac{h}{2}}^{\frac{h}{2}}\rho_h\Psi(z)[1,z]dz\\+&\int_{\frac{h}{2}}^{\frac{h}{2}+h_P}\rho_T\Psi(z)[1,z]dz+\int_{-(\frac{h}{2}+h_P)}^{-\frac{h}{2}}\rho_T\Psi(z)[1,z]dz\end{aligned} \quad (27)$$

$$I_5=\int_{-\frac{h}{2}}^{\frac{h}{2}}\rho_h\Psi^2(z)dz+\int_{\frac{h}{2}}^{\frac{h}{2}+h_P}\rho_T\Psi^2(z)dz \quad (28)$$

$$+\int_{-(\frac{h}{2}+h_P)}^{-\frac{h}{2}} \rho_T \Psi^2(z)dz$$

Using Eq. (16) and, Eqs. (17-20) solving the relationship and factorization, the equilibrium equation results in the following effect:

$$\begin{aligned}
&\delta u_0: \frac{dN_x}{dx} = I_0\ddot{u}_0 - I_1\frac{d\ddot{w}_0}{dx} + I_3\left(\frac{d\ddot{w}_0}{dx} - \ddot{\phi}_0\right)\\
&\delta w_0: \frac{d^2P_x}{dx^2} - \frac{d^2M_x}{dx^2} + \frac{dQ_x}{dx} + k_w w_0 - k_s\frac{d^2w_0}{dx^2}\\
&-f - N_{x0}\frac{d^2w_0}{dx^2} = I_0\ddot{w}_0 - I_1\frac{d\ddot{u}_0}{dx} + I_2\frac{d^2\ddot{w}_0}{dx^2}\\
&+I_3\frac{d\ddot{u}_0}{dx} + I_4(\frac{d\ddot{\phi}_0}{dx} - 2\frac{d^2\ddot{w}_0}{dx^2}) + I_5(\frac{d^2\ddot{w}_0}{dx^2} - \frac{d\ddot{\phi}_0}{dx})\\
&\delta\phi_0: -\frac{dP_x}{dx} - Q_x = -I_3\ddot{u}_0 + I_4\frac{d\ddot{w}_0}{dx} - I_5(\frac{d\ddot{w}_0}{dx} - \ddot{\phi}_0)
\end{aligned} \tag{29}$$

From the above relations, all stress resultants can be written in the form of material stiffness components and displacements as follows:

$$N_x = A_{11}\frac{du_0}{dx} - B_{11}\frac{d^2w_0}{dx^2} + C_{110}(\frac{d^2w_0}{dx^2} - \frac{d\phi_0}{dx}) \tag{30}$$

$$M_x = B_{11}\frac{du_0}{dx} - D_{11}\frac{d^2w_0}{dx^2} + E_{110}(\frac{d^2w_0}{dx^2} - \frac{d\phi_0}{dx}) \tag{31}$$

$$P_x = C_{110}\frac{du_0}{dx} - E_{110}\frac{d^2w_0}{dx^2} + H_{11}(\frac{d^2w_0}{dx^2} - \frac{d\phi_0}{dx}) \tag{32}$$

$$Q_x = A_{55}(\frac{dw_0}{dx} - \phi_0) \tag{33}$$

where:

$$\begin{aligned}
&[A_{11}, B_{11}, D_{11}] = \int_{-\frac{h}{2}}^{\frac{h}{2}} E_{11}[1, z, z^2]dz\\
&+\int_{\frac{h}{2}}^{\frac{h}{2}+h_P} C_{11}[1, z, z^2]dz + \int_{-(\frac{h}{2}+h_P)}^{-\frac{h}{2}} C_{11}[1, z, z^2]dz
\end{aligned} \tag{34}$$

$$\begin{aligned}
&[C_{110}, E_{110}] = \int_{-\frac{h}{2}}^{\frac{h}{2}} E_{11}\Psi(z)[1, z]dz\\
&+\int_{\frac{h}{2}}^{\frac{h}{2}+h_P} C_{11}\Psi(z)[1, z]dz + \int_{-(\frac{h}{2}+h_P)}^{-\frac{h}{2}} C_{11}\Psi(z)[1, z]dz
\end{aligned} \tag{35}$$

$$\begin{aligned}
&H_{11} = \int_{-\frac{h}{2}}^{\frac{h}{2}} E_{11}\Psi^2(z)dz\\
&+\int_{\frac{h}{2}}^{\frac{h}{2}+h_P} C_{11}\Psi^2(z)dz + \int_{-(\frac{h}{2}+h_P)}^{-\frac{h}{2}} C_{11}\Psi^2(z)dz
\end{aligned} \tag{36}$$

$$\begin{aligned}
&A_{55} = \int_{-\frac{h}{2}}^{\frac{h}{2}} Q_{55}(\frac{d\Psi(z)}{dz})^2dz\\
&+\int_{\frac{h}{2}}^{\frac{h}{2}+h_P} Q_{55}^T(\frac{d\Psi(z)}{dz})^2dz + \int_{-(\frac{h}{2}+h_P)}^{-\frac{h}{2}} Q_{55}^T(\frac{d\Psi(z)}{dz})^2dz
\end{aligned} \tag{37}$$

The stress resultants of Eqs. (30-33) are substituted into Eq. (29) to obtain the equations of motion or the governing equations in the form of displacements as follows:

$$\begin{aligned}
&A_{11}\frac{d^2u_0}{dx^2} - B_{11}\frac{d^3w_0}{dx^3} + C_{110}\left(\frac{d^3w_0}{dx^3} - \frac{d^2\phi_0}{dx^2}\right)\\
&= I_0\ddot{u}_0 - I_1\frac{d\ddot{w}_0}{dx} + I_3(\frac{d\ddot{w}_0}{dx} - \ddot{\phi}_0)
\end{aligned} \tag{38}$$

$$\begin{aligned}
&C_{110}\frac{d^3u_0}{dx^3} - E_{110}\frac{d^4w_0}{dx^4} + H_{11}\left(\frac{d^4w_0}{dx^4} - \frac{d^3\phi_0}{dx^3}\right)\\
&-B_{11}\frac{d^3u_0}{dx^3} + D_{11}\frac{d^4w_0}{dx^4} - E_{110}\left(\frac{d^4w_0}{dx^4} - \frac{d^3\phi_0}{dx^3}\right) +\\
&A_{55}\left(\frac{d^2w_0}{dx^2} - \frac{d\phi_0}{dx}\right) + k_w w_0\\
&-k_s\frac{d^2w_0}{dx^2} - f - N_{x0}\frac{d^2w_0}{dx^2}\\
&= I_0\ddot{w}_0 - I_1\frac{d\ddot{u}_0}{dx} + I_2\frac{d^2\ddot{w}_0}{dx^2} + I_3\frac{d\ddot{u}_0}{dx}\\
&+I_4(\frac{d\ddot{\phi}_0}{dx} - 2\frac{d^2\ddot{w}_0}{dx^2}) + I_5(\frac{d^2\ddot{w}_0}{dx^2} - \frac{d\ddot{\phi}_0}{dx})
\end{aligned} \tag{39}$$

$$\begin{aligned}
&-C_{110}\frac{d^2u_0}{dx^2} + E_{110}\frac{d^3w_0}{dx^3} - H_{11}\left(\frac{d^3w_0}{dx^3} - \frac{d^2\phi_0}{dx^2}\right)\\
&-A_{55}(\frac{dw_0}{dx} - \phi_0) = -I_3\ddot{u}_0 + I_4\frac{d\ddot{w}_0}{dx} - I_5(\frac{d\ddot{w}_0}{dx} - \ddot{\phi}_0)
\end{aligned} \tag{40}$$

2.4 Analytical solution

The following is used to discretization the relationships of the following assumptions. Therefore:

$$u_0(x,t) = \sum_{n=1}^{\infty} U_n(t)\,cos(\frac{n\pi x}{L}) \tag{41}$$

$$\phi_0(x,t) = \sum_{n=1}^{\infty} \Phi_n(t)\,cos(\frac{n\pi x}{L}) \tag{42}$$

$$w_0(x,t) = \sum_{n=1}^{\infty} W_n(t)\,sin(\frac{n\pi x}{L}) \tag{43}$$

$U_n(t)$, $W_n(t)$ and $\Phi_n(t)$ are the unknown Fourier coefficients to be determined for each *n* value. By using the general property of the Dirac Delta function as follows:

$$\begin{aligned}
&\delta(x - V_1t) = 2\sum_{n=1}^{\infty} sin(\frac{n\pi x}{L})\,sin(\frac{n\pi V_1 t}{L})\\
&\delta(x - V_2t) = 2\sum_{n=1}^{\infty} sin(\frac{n\pi x}{L})\,sin(\frac{n\pi V_2 t}{L})
\end{aligned} \tag{44}$$

Assuming:

$$\alpha = (\frac{n\pi}{L})$$

With the initial condition:

$$\begin{aligned}
&W_n(0) = \dot{W}_n(0) = U_n(0) = \dot{U}_n(0)\\
&= \Phi_n(0) = \dot{\Phi}_n(0) = 0
\end{aligned} \tag{45}$$

To solve the system of the differential Eqs. (38), (39), and (40) in the time domain, Laplace transform is utilized. By recalling this transform as follows:

$$\begin{matrix} L\left[\ddot{W}_n(t)\right] = s^2W_n(s) - sW_n(0) - \dot{W}_n(0), W_n(s) = L[W_n(t)] \\ L\left[\ddot{U}_n(t)\right] = s^2U_n(s) - sU_n(0) - \dot{U}_n(0), U_n(s) = L[U_n(t)] \\ L\left[\ddot{\Phi}_n(t)\right] = s^2\Phi_n(s) - s\Phi_n(0) - \dot{\Phi}_n(0), \Phi_n(s) = L[\Phi_n(t)] \end{matrix} \quad (46)$$

where applying Laplace Transform in Eqs. (38), (39), and (40), the system of equation is obtained as follows:

$$\begin{pmatrix} K_{11} & K_{12} & K_{13} \\ K_{21} & K_{22} & K_{23} \\ K_{31} & K_{32} & K_{33} \end{pmatrix} \begin{Bmatrix} U_n(s) \\ W_n(s) \\ \Phi_n(s) \end{Bmatrix} = \begin{Bmatrix} 0 \\ F \\ 0 \end{Bmatrix} \quad (47)$$

where:

$$\begin{matrix} A_{11}\alpha^2 + I_0s^2, \\ K_{12} = K_{21} = B_{11}\alpha^3 - C_{110}\alpha^3 + I_1\alpha s^2 - I_3\alpha s^2, \\ K_{13} = K_{31} = C_{110}\alpha^2 + I_3s^2 \\ K_{22} = -2E_{110}\alpha^4 + H_{11}\alpha^4 + D_{11}\alpha^4 \\ +A_{55}\alpha^2 + k_w + k_s\alpha^2 - N_{x0}\alpha^2 \\ +I_0s^2 + I_2\alpha^2s^2 - 2I_4\alpha^2s^2 + I_5\alpha^2s^2 \\ K_{23} = K_{32} = -H_{11}\alpha^3 + E_{110}\alpha^3 \\ -A_{55}\alpha + I_4\alpha s^2 - I_5\alpha s^2, \\ K_{33} = H_{11}\alpha^2 + A_{55} + I_5s^2 \\ F = \frac{2P_1(\alpha V_1)}{s^2 + (\alpha V_1)^2} + \frac{P_2(\omega + \alpha V_2)}{s^2 + (\omega + \alpha V_2)^2} \\ + \frac{P_2(\omega - \alpha V_2)}{s^2 + (\omega - \alpha V_2)^2} \end{matrix} \quad (48)$$

By solving the Eq. (47), $U_n(s)$, $W_n(s)$ and $\Phi_n(s)$ are obtained as:

$$\begin{matrix} \begin{pmatrix} U_n(s) \\ W_n(s) \\ \Phi_n(s) \end{pmatrix} = \frac{1}{det(K)} \begin{pmatrix} F(-K_{13}K_{23} + K_{12}K_{33}) \\ F\left({K_{13}}^2 - K_{11}K_{33}\right) \\ -F(K_{12}K_{13} - K_{11}K_{23}) \end{pmatrix} \\ det(K) = {K_{13}}^2K_{22} - 2K_{12}K_{13}K_{23} + K_{11}{K_{23}}^2 + {K_{12}}^2K_{33} \\ - K_{11}K_{22}K_{33} \end{matrix} \quad (49)$$

By applying in inverse Laplace transform to Eq. (49), the transverse and axial dynamic responses of the thermoelectric CNTRC beam are obtained:

$$\begin{matrix} U_n(x,t) = \frac{1}{y_2}\left(\frac{y_1 sin\left[\sqrt{d_{18}}t\right]}{\sqrt{d_{18}}}\right) + \frac{1}{y_4}\left(\frac{y_3 sin\left[\sqrt{d_{20}}t\right]}{\sqrt{d_{20}}}\right) \\ + \frac{1}{y_6}\left(\frac{y_5 sin\left[\sqrt{d_{22}}t\right]}{\sqrt{d_{22}}}\right) + \\ \frac{\begin{pmatrix} -g_6\left(f_0 + x_1(f_2 + f_4x_1)\right)\sqrt{x_2}(x_2 - x_3)\sqrt{x_3}\, sinh[t\sqrt{x_1}] + \\ g_6\sqrt{x_1}\left(\left(f_0 + x_2(f_2 + f_4x_2)\right)(x_1 - x_3)\sqrt{x_3}\, sinh[t\sqrt{x_2}] + \\ \sqrt{x_2}(-x_1 + x_2)\left(f_0 + x_3(f_2 + f_4x_3)\right) sinh\left[t\sqrt{x_3}\right]\right) \end{pmatrix}}{\sqrt{x_1}\sqrt{x_2}\sqrt{x_3}\left(g_2g_4 - 3g_0g_6 + 2{g_6}^2(x_1{x_2}^2 + {x_1}^2x_3 + x_2{x_3}^2)\right)} \end{matrix} \quad (50)$$

$$\begin{matrix} W_n(x,t) = \frac{1}{y_2}\left(\frac{y_7 sin\left[\sqrt{d_{18}}t\right]}{\sqrt{d_{18}}}\right) + \frac{1}{y_4}\left(\frac{y_8 sin\left[\sqrt{d_{20}}t\right]}{\sqrt{d_{20}}}\right) \\ + \frac{1}{y_6}\left(\frac{y_9 sin\left[\sqrt{d_{22}}t\right]}{\sqrt{d_{22}}}\right) + \\ \frac{\begin{pmatrix} -g_6\left(J_0 + x_1(J_2 + J_4x_1)\right)\sqrt{x_2}(x_2 - x_3)\sqrt{x_3}\, sinh[t\sqrt{x_1}] + \\ g_6\sqrt{x_1}\left(\left(J_0 + x_2(J_2 + J_4x_2)\right)(x_1 - x_3)\sqrt{x_3}\, sinh[t\sqrt{x_2}] + \\ \sqrt{x_2}(-x_1 + x_2)\left(J_0 + x_3(J_2 + J_4x_3)\right) sinh\left[t\sqrt{x_3}\right]\right) \end{pmatrix}}{\sqrt{x_1}\sqrt{x_2}\sqrt{x_3}\left(g_2g_4 - 3g_0g_6 + 2{g_6}^2(x_1{x_2}^2 + {x_1}^2x_3 + x_2{x_3}^2)\right)} \end{matrix} \quad (51)$$

$$\begin{matrix} \Phi_n(x,t) = \frac{1}{y_2}\left(\frac{y_{10} sin\left[\sqrt{d_{18}}t\right]}{\sqrt{d_{18}}}\right) + \frac{1}{y_4}\left(\frac{y_{11} sin\left[\sqrt{d_{20}}t\right]}{\sqrt{d_{20}}}\right) \\ + \frac{1}{y_6}\left(\frac{y_{12} sin\left[\sqrt{d_{22}}t\right]}{\sqrt{d_{22}}}\right) + \\ \frac{\begin{pmatrix} -g_6\left(R_0 + x_1(R_2 + R_4x_1)\right)\sqrt{x_2}(x_2 - x_3)\sqrt{x_3}\, sinh[t\sqrt{x_1}] + \\ g_6\sqrt{x_1}\left(\left(R_0 + x_2(R_2 + R_4x_2)\right)(x_1 - x_3)\sqrt{x_3}\, sinh[t\sqrt{x_2}] + \\ \sqrt{x_2}(-x_1 + x_2)\left(R_0 + x_3(R_2 + R_4x_3)\right) sinh\left[t\sqrt{x_3}\right]\right) \end{pmatrix}}{\sqrt{x_1}\sqrt{x_2}\sqrt{x_3}\left(g_2g_4 - 3g_0g_6 + 2{g_6}^2(x_1{x_2}^2 + {x_1}^2x_3 + x_2{x_3}^2)\right)} \end{matrix} \quad (52)$$

3. Analytical results and discussions

The results presented in this chapter are related to analyzing the axial and transverse dynamic response of thermoelectric CNTRC beams under moving harmonic and constant load resting on the Pasternak foundation. Also, the influence of parameters such as excitation frequency, voltage, temperature, spring constant factors, the volume fraction of CNTs, and load velocity on the dynamic response of the thermoelectric CNTRC beams in axial and transverse modes was investigated.

The relations described in Eq. (53) are performed to calculate dimensionless natural frequencies.

$$\begin{matrix} V_{CNT} + V_m = 1 \left[\begin{pmatrix} s_{11} & s_{12} & s_{13} \\ s_{12} & s_{22} & s_{23} \\ s_{13} & s_{23} & s_{33} \end{pmatrix} - \lambda^2 \begin{pmatrix} m_{11} & m_{12} & m_{13} \\ m_{12} & m_{22} & m_{23} \\ m_{13} & m_{23} & m_{33} \end{pmatrix} \right] \begin{Bmatrix} U_n(s) \\ W_n(s) \\ \Phi_n(s) \end{Bmatrix} = \begin{Bmatrix} 0 \\ F \\ 0 \end{Bmatrix} \\ s_{11} = A_{11}\alpha^2,\ s_{12} = B_{11}\alpha^3 - C_{110}\alpha^3, \\ s_{13} = C_{110}\alpha^2, \\ s_{22} = -2E_{110}\alpha^4 + H_{11}\alpha^4 + D_{11}\alpha^4 \\ +A_{55}\alpha^2 + k_w + k_s\alpha^2 - N_{x0}\alpha^2, \\ s_{23} = -H_{11}\alpha^3 + E_{110}\alpha^3 - A_{55}\alpha, \\ s_{33} = H_{11}\alpha^2 + A_{55}, \qquad m_{11} = -I_0, \\ m_{12} = -I_1\alpha + I_3\alpha, \qquad m_{13} = -I_3, \\ m_{22} = -I_0 - I_2\alpha^2 + 2I_4\alpha^2 - I_5\alpha^2 \\ m_{23} = -I_4\alpha + I_5\alpha,\ m_{33} = -I_5, \\ \bar{\omega} = \lambda\frac{L^2}{h}\sqrt{\frac{\rho^k}{E^k}} \end{matrix} \quad (53)$$

The results are compared with (Wattanasakulpong and Ungbhakorn 2013), given in Table 1 and Table 2. Also, the dimensions of the beam are: $\frac{L}{h} = 100, L = 100, h_p = 0.1$.

As shown in Table 1, among different types of CNTRC beams, frequency O-Beam is the lowest, and X-Beam is the highest.

Figs. (2)-(5) shows the axial displacement in terms of time. Fig. 2 shows the axial displacements for different spring constant for V-Beam on elastic foundation versus time. As can be seen, with increasing spring constant, the axial displacement decrease.

Fig. 3 shows the axial displacements for different excitation frequencies for V-Beam on elastic foundation versus time. The moving harmonic force decreases with increasing excitation frequency, and the axial displacement decreases.

Table 1 Comparisons of fundamental frequencies for CNTRC beams with and without elastic foundation for HSDT $\frac{L}{h} = 15, V_{CN}^{*} = 0.12$

	UD-Beam	V-Beam	O-Beam	X-Beam
$\bar{\omega}_1$	0.974908	0.745672	1.11562	0.844435
$\bar{\omega}_1$ (Wattanasakulpong and Ungbhakorn 2013)	0.9745	0.7454	1.1151	0.8441
$\bar{\omega}_2$	2.88138	2.39797	3.10205	2.6492
$\bar{\omega}_3$	4.93056	4.29371	5.16984	4.68817
$\bar{\omega}_4$	7.01828	6.22862	7.2849	6.79126

Table 2 Compares displacements and stresses for isotropic beams without elastic foundation subjected to uniform load $\frac{L}{h} = 20$

	$\bar{w}$(Wattanasakulpong and Ungbhakorn 2013)	$\bar{w}$[Present]	$\bar{\sigma}_x$(Wattanasakulpong and Ungbhakorn 2013)	$\bar{\sigma}_x$[Present]	$\bar{\sigma}_{xz}$(Wattanasakulpong and Ungbhakorn 2013)	$\bar{\sigma}_{xz}$[Present]
HSDT	2.8962	2.8962	15.0131	15.0129	0.7402	0.7417

Table 3 Properties of PMMA and SWCNTs (10, 10) (Shen and Xiang 2013)

Material		Properties
PMMA	E^k(GPa)	2.5
	$\rho^k(\frac{\text{Kg}}{m^3})$	1190
	υ^k	0.3
	$\alpha^k(K^{-1})$	0.3×10^{-6}
SWCNTs	E_{11}^{CN}(GPa)	600
	G_{12}^{CN}(GPa)	17.2
	$\rho_{CN}(\frac{\text{Kg}}{m^3})$	1400
	υ_{CN}	0.19
	$\alpha_h(K^{-1})$	23×10^{-6}
	$d_{31}(\frac{m}{V})$	0.254

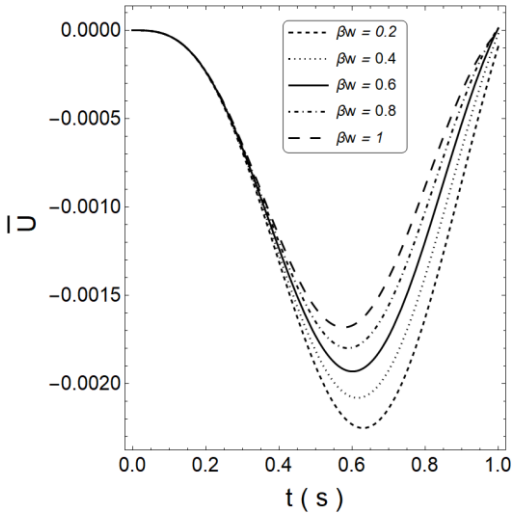

Fig. 2 Variation of dimensionless axial dynamic deflection V-Beam on Pasternak foundation versus time for different spring constant of moving load $V_1 = 10, V_2 = 20, \frac{L}{h} = 100, \beta_s = 0.02, \Delta T$=10,$V_{CN}^{*} = 0.12, \omega = 3$

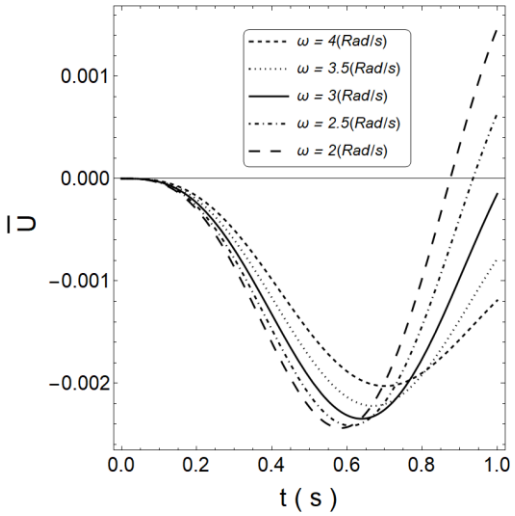

Fig. 3 Variation of dimensionless axial dynamic deflection V-Beam on Pasternak foundation versus time for different excitation frequency of moving load $V_1 = 10, V_2 = 20, \frac{L}{h} = 100, \beta_w = 0.1, \beta_s = 0.02, \Delta T$=10,$V_{CN}^{*} = 0.12$

Fig. 4 shows the axial displacements for different temperatures for V-Beam on elastic foundation versus time. As can be seen, with increasing temperature, the axial displacement also increases.

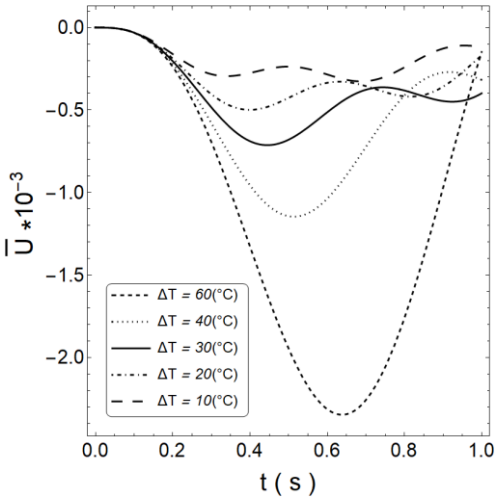

Fig. 4 Variation of dimensionless axial dynamic deflection V-Beam on Pasternak foundation versus time for the different temperatures of moving load $V_1 = 10,\ V_2 = 20,\ \frac{L}{h} = 100,\ \beta_w = 0.1,\ \beta_s = 0.02,$ voltage = 0, $V_{CN}^* = 0.12,\ \omega = 3$

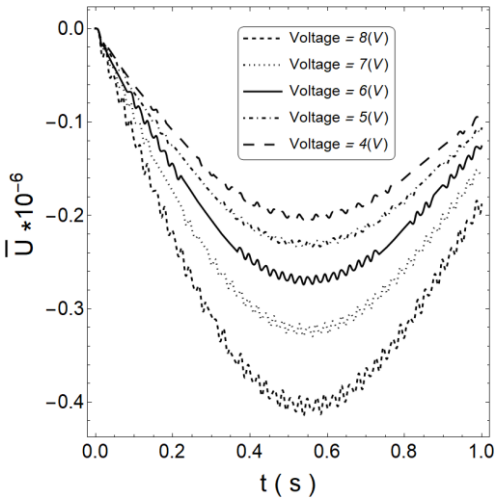

Fig. 5 Variation of dimensionless axial dynamic deflection V-Beam on Pasternak foundation versus time for different voltage of moving load $V_1 = 10, V_2 = 20, \frac{L}{h} = 100, \beta_w = 0.1,\ \beta_s = 0.02,\ \Delta T$=0, $V_{CN}^* = 0.12,\ \omega = 3$

Fig. 5 shows the axial displacements for the different voltage for V-Beam on elastic foundation versus time. With increasing voltage, the axial displacement increases.

Fig. 6 shows the axial displacements for the different velocities of constant load for V-Beam on elastic foundation versus time. As can be seen, the axial displacement increases with the increasing velocity of the constant load.

Fig. 7 shows the axial displacements for the different velocities of harmonic for V-Beam on elastic foundation versus time and temperature. As can be seen, with increasing harmonic velocity, the axial displacement decreases, and with increasing temperature, the axial displacement also increases.

Figs. (8)-(11) shows the transverse displacement in terms of time. Fig. 8 shows the axial displacements for

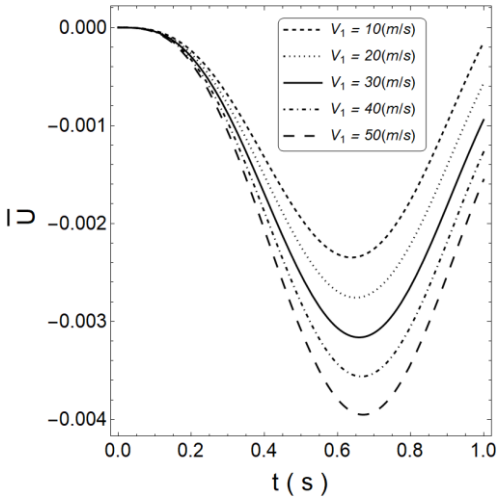

Fig. 6 Variation of dimensionless axial dynamic deflection V-Beam on Pasternak foundation versus time for the different velocity of constant load $V_2 = 20,\ \frac{L}{h} = 100,\ \beta_w = 0.1,\ \beta_s = 0.02,\ \Delta T$=10, $V_{CN}^* = 0.12,\ \omega = 3$

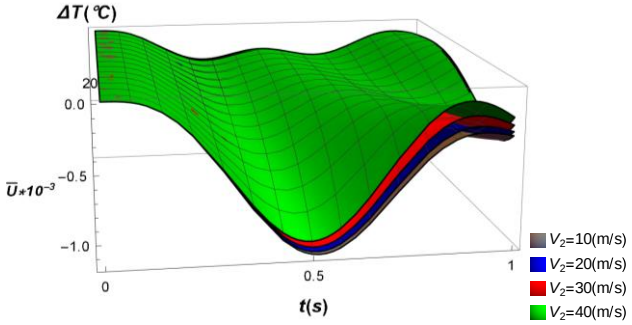

Fig. 7 Variation of dimensionless axial dynamic deflection V-Beam on Pasternak foundation versus time and temperature for the different velocity of harmonic load $V_1 = 10,\ \frac{L}{h} = 100,\ \beta_w = 0.1,\ \beta_s = 0.02,$ voltage = 0, $V_{CN}^* = 0.12,\ \omega = 3$

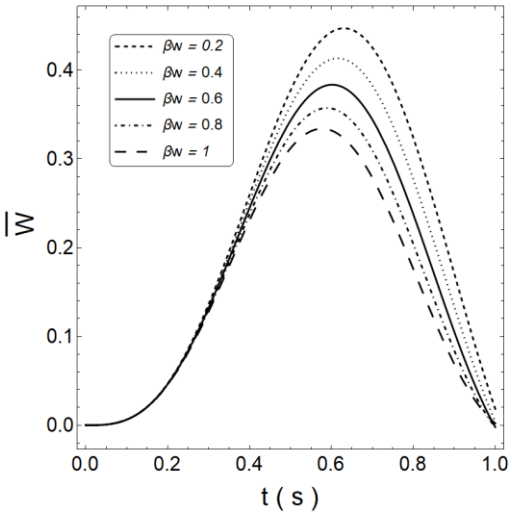

Fig. 8 Variation of dimensionless transverse dynamic deflection V-Beam on Pasternak foundation versus time for different spring constant of moving load $V_1 = 10,\ V_2 = 20,\ \frac{L}{h} = 100,\ \beta_s = 0.02,\ \Delta T$=10, $V_{CN}^* = 0.12,\ \omega = 3$

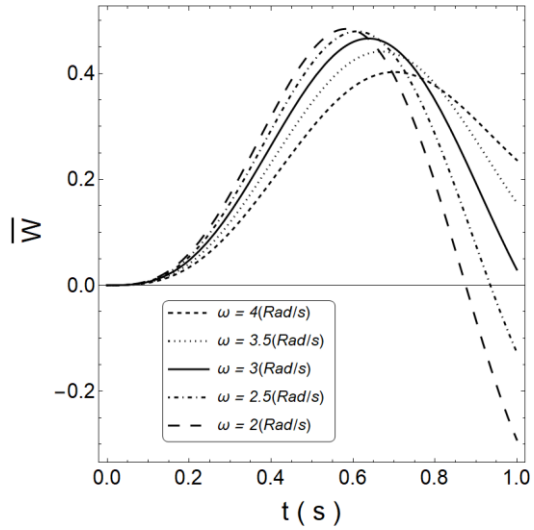

Fig. 9 Variation of dimensionless transverse dynamic deflection V-Beam on Pasternak foundation versus time for different excitation frequency of moving load $V_1 = 10,\ V_2 = 20,\ \frac{L}{h} = 100,\ \beta_w = 0.1,\ \beta_s = 0.02,\ \Delta T$=10, $V_{CN}^* = 0.12$

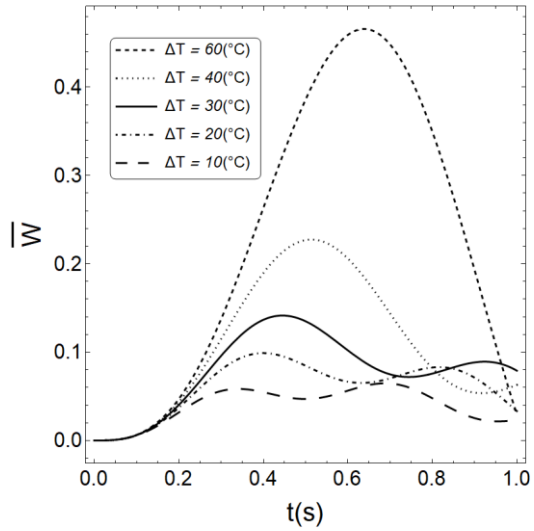

Fig. 10 Variation of dimensionless transverse dynamic deflection V-Beam on Pasternak foundation versus time for the different temperatures of moving load $V_1 = 10, V_2 = 20,\ \frac{L}{h} = 100,\ \beta_w = 0.1,\ \beta_s = 0.02,$ voltage = 0, $V_{CN}^* = 0.12,\ \omega = 3$

different spring constant for V-Beam on elastic foundation versus time. As can be seen, with increasing spring constant, the transverse displacement decrease.

Fig. 9 shows the transverse displacements for different excitation frequencies for V-Beam on elastic foundation versus time. The moving harmonic force decreases with increasing excitation frequency, and the transverse displacement decreases.

Fig. 10 shows the transverse displacements for different temperatures for V-Beam on elastic foundation versus time. As can be seen, the transverse displacement also increases with increasing temperature.

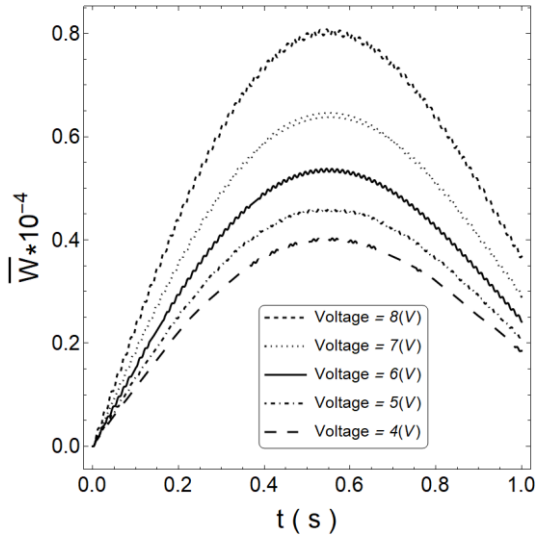

Fig. 11 Variation of dimensionless transverse dynamic deflection V-Beam on Pasternak foundation versus time for different voltage of moving load $V_1 = 10,\ V_2 = 20,\ \frac{L}{h} = 100,\ \beta_w = 0.1,\ \beta_s = 0.02,\ \Delta T$=0, $V_{CN}^* = 0.12,\ \omega = 3$

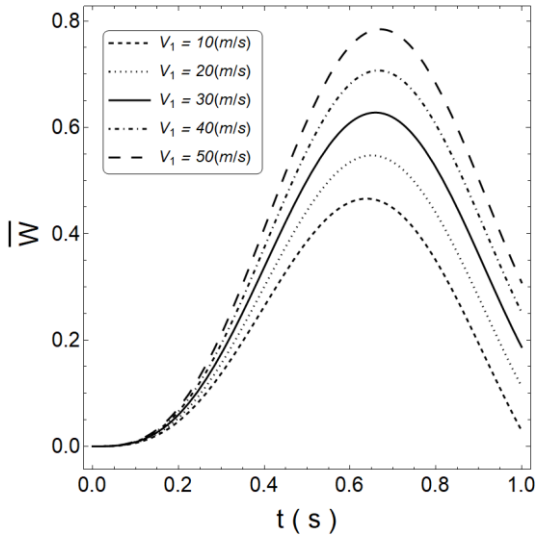

Fig. 12 Variation of dimensionless transverse dynamic deflection V-Beam on Pasternak foundation versus time for the different velocity of constant load $V_2 = 20,\ \frac{L}{h} = 100,\ \beta_w = 0.1,\ \beta_s = 0.02,\ \Delta T$=10, $V_{CN}^* = 0.12,\ \omega = 3$

Fig. 11 shows the transverse displacements for the different voltage for V-Beam on elastic foundation versus time. With increasing voltage, the transverse displacement increases.

Fig. 12 shows the transverse displacements for different velocities of constant load for V-Beam on elastic foundation versus time, as can be seen, the transverse displacement increases with the increasing velocity of constant load.

Fig. 13 shows the transverse displacements for different temperatures for V-Beam on elastic foundation versus time and spring constant as can be seen, with increasing temperature, the transverse displacement increase, and with increasing spring constant, the transverse displacement decrease.

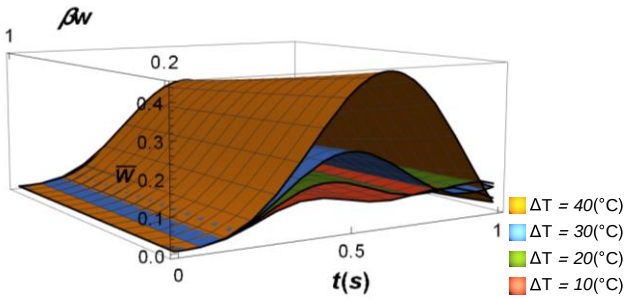

Fig. 13 Variation of dimensionless transverse dynamic deflection V-Beam on Pasternak foundation versus time and spring constant for the different temperatures of moving load $V_1 = 10,\ \frac{L}{h} = 100,\ \beta_w = 0.1,\ \beta_s = 0.02,$ voltage = 0, $V_{CN}^* = 0.12,\ \omega = 3$

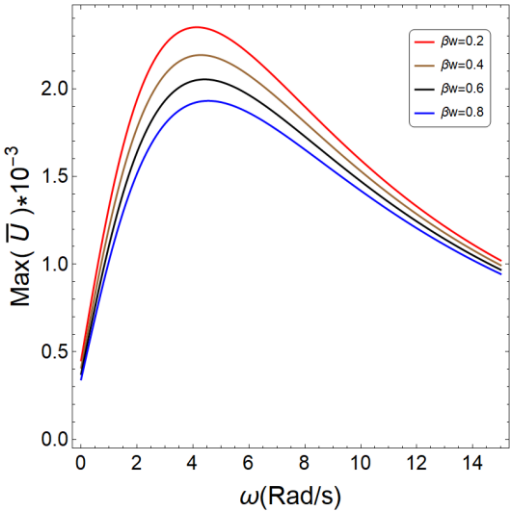

Fig. 14 Maximum dimensionless axial displacements of V-Beam on Pasternak foundation under moving load versus excitation frequency for different spring constant

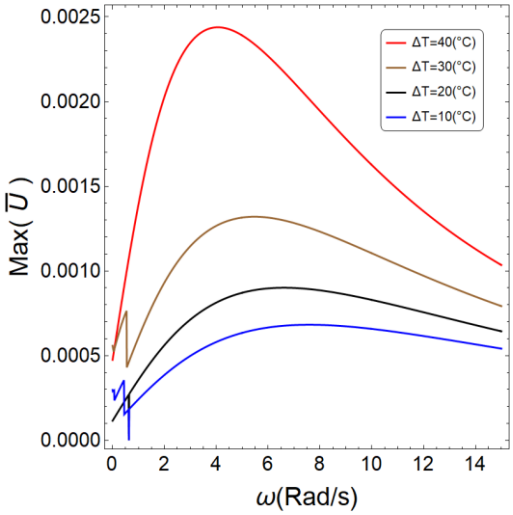

Fig. 15 Maximum dimensionless axial displacements of V-Beam on Pasternak foundation under moving load versus excitation frequency for different temperature

In Fig. 16, maximum dimensionless transverse displacements of V-Beam on elastic foundation under moving load versus excitation frequency for different spring constant shows. By increasing the spring constant, maximum dimensionless transverse displacements decrease.

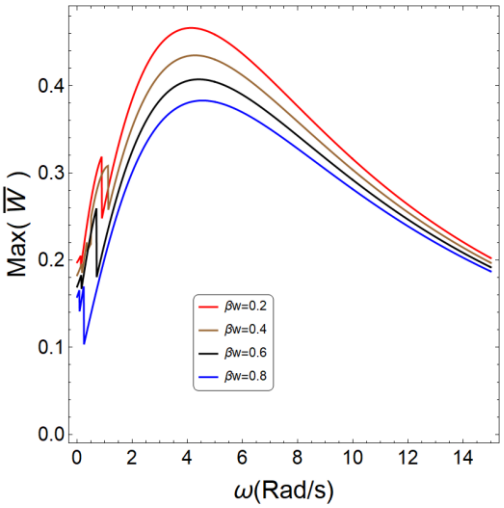

Fig. 16 Maximum dimensionless transverse displacements of V-Beam on Pasternak foundation under moving load versus excitation frequency for different spring constant $V_1 = 10,\ V_2 = 20,\ \frac{L}{h} = 100,\ \beta_s = 0.02, \Delta\ T$=10, $V_{CN}^* = 0.12$

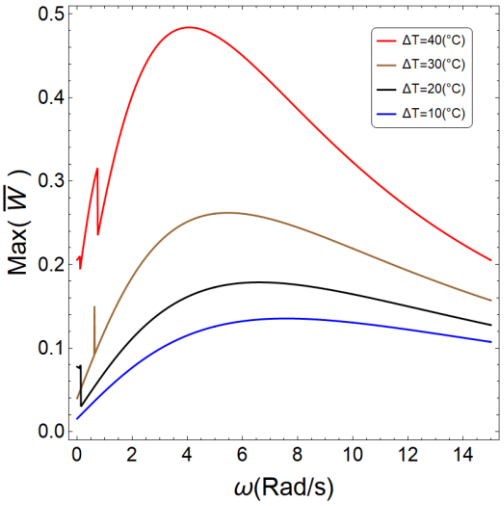

Fig. 17 Maximum dimensionless transverse displacements of V-Beam on Pasternak foundation under moving load versus excitation frequency for different temperature $V_1 = 10,\ V_2 = 20,\ \frac{L}{h} = 100,\ \beta_w = 0.1,\ \beta_s = 0.02,\ voltage = 0,\ V_{CN}^* = 0.12$

In Fig. 17, maximum dimensionless transverse displacements of V-Beam on elastic foundation under moving load versus excitation frequency for different temperature shows. By increasing the temperature, maximum dimensionless transverse displacements increase.

Fig. 18 maximum dimensionless transverse displacements of CNTRC beams on elastic foundation under moving load versus excitation frequency. As can be seen, beams O, V, UD, and X have the highest max transverse dynamic deflection, respectively.

In Fig. 19, maximum dimensionless transverse displacements of V-Beam on elastic foundation under moving load

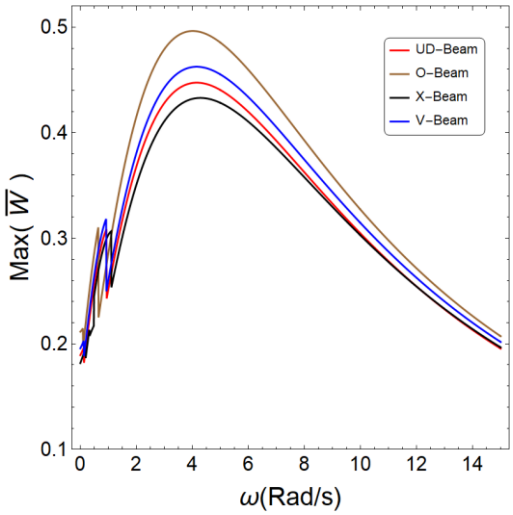

Fig. 18 Maximum dimensionless transverse displacements of CNTRC beams on Pasternak foundation under moving load versus excitation frequency $V_1 = 10$, $V_2 = 20$, $\frac{L}{h} = 100$, $\beta_w = 0.1$, $\beta_s = 0.02$, $Voltage = 0, V_{CN}^* = 0.12$, $\Delta T = 10$

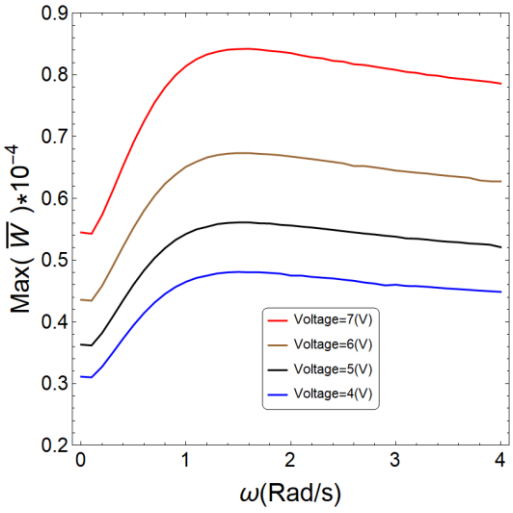

Fig. 19 Maximum dimensionless transverse displacements of V-Beam on Pasternak foundation under moving load versus excitation frequency for different voltage $V_1 = 10, V_2 = 20$, $\frac{L}{h} = 100$, $\beta_w = 0.1$, $\beta_s = 0.02$, $\Delta T = 0$, $V_{CN}^* = 0.12$

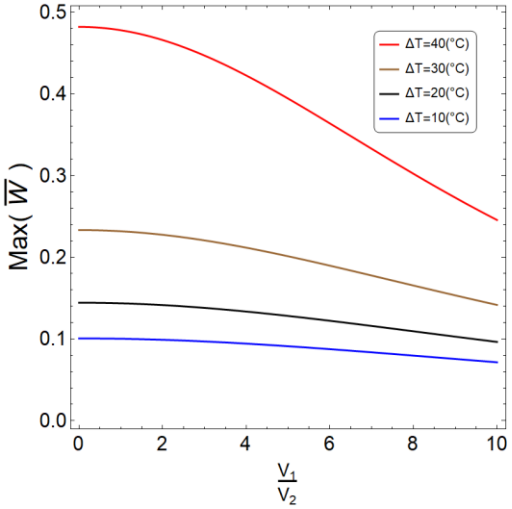

Fig. 20 Maximum dimensionless transverse displacements of V-Beam on Pasternak foundation under moving load versus constant velocity to harmonic velocity ratio for different temperature $V_1 = 10$, $V_2 = 20$, $\frac{L}{h} = 100$, $\beta_w = 0.1$, $\beta_s = 0.02$, $voltage = 0$, $V_{CN}^* = 0.12$

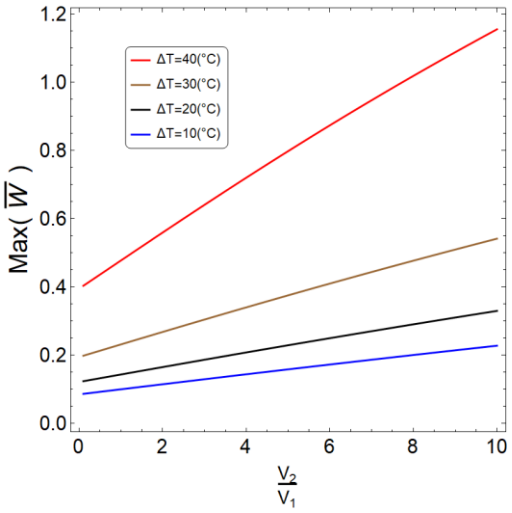

Fig. 21 Maximum dimensionless transverse displacements of V-Beam on Pasternak foundation under moving load versus harmonic velocity to constant velocity ratio for different temperature $V_1 = 10$, $V_2 = 20$, $\frac{L}{h} = 100$, $\beta_w = 0.1$, $\beta_s = 0.02$, $voltage = 0$, $V^*_{CN} = 0.12$

versus excitation frequency for different voltage shows. By increasing the voltage, maximum dimensionless transverse displacements increase.

In Fig. 20, maximum dimensionless transverse displacements of V-Beam on elastic foundation under moving load versus constant velocity to harmonic velocity ratio for different temperatures. Maximum dimensionless transverse displacements decrease by increasing constant velocity to harmonic velocity ratio. Increasing the harmonic velocity reduces the maximum dimensionless transverse displacement.

In Fig. 21, maximum dimensionless transverse displacements of V-Beam on elastic foundation under moving load versus harmonic velocity to constant velocity ratio for different temperatures. The maximum dimension-less transverse displacements increase harmonic velocity to constant velocity ratio. Increasing the constant velocity increases the maximum dimensionless transverse displacement.

4. Conclusions

This study analyzes the axial and transverse dynamic response of CNTRC beams on the Pasternak foundation under moving harmonic and constant load. The governing equations of the CNTRC beam are obtained based on higher-order shear deformation theory, Hamilton principle, and Laplace transforms to solve the derived differential equations.

Based on the analytical results, it was found that the parameters of beam thickness, excitation frequency temperature changes, voltage, spring constant, and moving load speed have a significant effect on forced vibrations and transverse and axial displacement of CNTRC beams.

Among CNTRC beams, the highest transverse and axial displacement are for O, V, UD, and X beams, respectively. Maximum dimensionless transverse displacements of CNTRC beams on elastic foundation under moving load versus excitation frequency. Beams O, V, UD, and X have the highest max transverse dynamic deflection, respectively, so O-Beam has the weakest resistance to flexural loads. Also, among different CNTRC beams, frequency O-Beam is the lowest, and X-Beam is the highest. They increased the aspect ratio of the transverse and axial displacement of the CNTRC beams. Also, by increasing the excitation frequency V_{CN}^{*}, the transverse and axial displacement of the CNTRC beams is reduced.

The axial displacement diagram has values for the states where the arrow is close to state FG and zero for other states, for example, UD-Beam.

It increases the voltage, temperature, and aspect ratio of the transverse displacement of the CNTRC beams, and bending increases.

Increasing the spring constant, velocity, and transverse displacement of the CNTRC beams and bending is reduced.

As the velocity of the moving constant load increases, the transverse and axial displacements increase. With increasing the velocity of the moving harmonic load, the transverse and axial displacements decrease.

References

Abdelrahman, A.A., Esen, I., Daikh, A.A. and Eltaher, M.A. (2021), "Dynamic analysis of FG nanobeam reinforced by carbon nanotubes and resting on elastic foundation under moving load", *Mech. Based Des. Struct.*, 1-24. https://doi.org/10.1080/15397734.2021.1999263

Alazwari, M.A., Daikh, A.A., Houari, M.S.A., Tounsi, A. and Eltaher, M.A. (2021), "On static buckling of multilayered carbon nanotubes reinforced composite nanobeams supported on non-linear elastic foundations", *Steel Compos. Struct.*, **40**(3), 389-404. https://doi.org/10.12989/scs.2021.40.3.389

Alizade Hamidi, B., Hosseini, S.A.H., Hassannejad, R. and Khosravi, F. (2019), "An exact solution on gold microbeam with thermoelastic damping via generalized Green-Naghdi and modified couple stress theories", *J. Therm. Stress.*, **43**(2), 157-174. https://doi.org/1010.1080/01495739.2019.1666694

Alizadeh-Hamidi, B., Hassannejad, R. and Omidi, Y. (2021), "Size-dependent thermo-mechanical vibration of lipid supramolecular nano-tubules via nonlocal strain gradient Timoshenko beam theory", *Comput. Biol. Med.*, **134**, 104475. https://doi.org/10.1016/j.compbiomed.2021.104475

Alizadeh Hamidi, B., Khosravi, F., Hosseini, S.A. and Hassannejad, R. (2020), "Closed form solution for dynamic analysis of rectangular nanorod based on nonlocal strain gradient", *Waves Random Complex Med.*, 1-17. https://doi.org/10.1080/17455030.2020.1843737

Babaei, H. (2022), "Free vibration and snap-through instability of FG-CNTRC shallow arches supported on nonlinear elastic foundation", *Appl. Math. Comput.*, **413**, 126606. https://doi.org/10.1016/j.amc.2021.126606

Babaei, H., Kiani, Y. and Eslami, M.R. (2021a), "Vibrational behavior of thermally pre-/post-buckled FG-CNTRC beams on a nonlinear elastic foundation: a two-step perturbation technique", *Acta Mechanica*, **232**(10), 3897-3915. https://doi.org/10.1007/s00707-021-03027-z

Babaei, H., Kiani, Y. and Reza Eslami, M. (2021b), "Perturbation method for thermal post-buckling analysis of shear deformable FG-CNTRC beams with different boundary conditions", *Int. J. Struct. Stabil. Dyn.*, **21**(13), 2150175. https://doi.org/10.1142/S0219455421501753

Behrouz, S.J., Rahmani, O. and Hosseini, S.A. (2019), "On nonlinear forced vibration of nano cantilever-based biosensor via couple stress theory", *Mech. Syst. Signal Pr.*, **128**, 19-36. https://doi.org/10.1016/j.ymssp.2019.03.020

Bensattalah, T., Daouadji, T., Zidour, M., Tounsi, A. and Bedia, E. (2016), "Investigation of thermal and chirality effects on vibration of single-walled carbon nanotubes embedded in a polymeric matrix using nonlocal elasticity theories", *Mech. Compos. Mater.*, **52**(4), 555-568. https://doi.org/10.1007/s11029-016-9606-z

Bensattalah, T., Hamidi, A., Bouakkaz, K., Zidour, M. and Daouadji, T.H. (2020), "Critical buckling load of triple-walled carbon nanotube based on nonlocal elasticity theory", *J. Nano Res.*, **62**, 108-119. https://doi.org/10.4028/www.scientific.net/JNanoR.62.108

Bensattalah, T., Zidour, M., Daouadji, T.H. and Bouakaz, K. (2019), "Theoretical analysis of chirality and scale effects on critical buckling load of zigzag triple walled carbon nanotubes under axial compression embedded in polymeric matrix", *Struct. Eng. Mech.*, **70**(3), 269-277. https://doi.org/10.12989/sem.2019.70.3.269

Boulal, A., Bensattalah, T., Karas, A., Zidour, M., Heireche, H. and Bedia, E.A. (2020), "Buckling of carbon nanotube reinforced composite plates supported by Kerr foundation using Hamilton's energy principle", *Struct. Eng. Mech.*, **73**(2), 209-223. https://doi.org/10.12989/sem.2020.73.2.209

Chalak, H., Zenkour, A. and Garg, A. (2021), "Free vibration and modal stress analysis of FG-CNTRC beams under hygrothermal conditions using zigzag theory", *Mech. Based Des. Struct.*, 1-22. https://doi.org/10.1080/15397734.2021.1977659

Civalek, Ö., Akbaş, Ş.D., Akgöz, B. and Dastjerdi, S. (2021a), "Forced vibration analysis of composite beams reinforced by carbon nanotubes", *Nanomaterials*. **11**(3), 571. https://doi.org/10.3390/nano11030571

Civalek, Ö., Dastjerdi, S., Akbaş, Ş.D. and Akgöz, B. (2021b), "Vibration analysis of carbon nanotube-reinforced composite microbeams", *Math. Meth. Appl. Sci.*, Special Issue Paper. https://doi.org/10.1002/mma.7069

Ebrahimi, F., Salari, E. and Hosseini, S. (2015), "In-plane thermal loading effects on vibrational characteristics of functionally graded nanobeams", *Meccanica*, 1-27. https://doi.org/10.1007/s11012-015-0248-3

Ebrahimi, F., Farazmandnia, N., Kokaba, M.R. and Mahesh, V. (2021a), "Vibration analysis of porous magneto-electro-elastically actuated carbon nanotube-reinforced composite sandwich plate based on a refined plate theory", *Eng. Comput.*, **37**(2), 921-936.https://doi.org/10.1007/s00366-019-00864-4

Ebrahimi, F., Seyfi, A. and Dabbagh, A. (2021b), "The effects of thermal loadings on wave propagation analysis of multi-scale hybrid composite beams", *Wave Random Complex Med.*, 1-24. https://doi.org/10.1080/17455030.2021.1956015

Ebrahimi, F., Seyfi, A. and Teimouri, A. (2021c), "Torsional vibration analysis of scale-dependent non-circular graphene oxide powder-strengthened nanocomposite nanorods", *Eng. Comput.*, 1-12. https://doi.org/10.1007/s00366-021-01528-y

Eghbali, M., Hosseini, S.A. and Rahmani, O. (2021), "Free vibration of axially functionally graded nanobeam with an

attached mass based on nonlocal strain gradient theory via new ADM numerical method", *Amirkabir J. Mech. Eng.*, **53**(2), 8-8. https://doi.org/10.22060/mej.2020.17013.6495

Gafour, Y., Hamidi, A., Benahmed, A., Zidour, M. and Bensattalah, T. (2020), "Porosity-dependent free vibration analysis of FG nanobeam using non-local shear deformation and energy principle", *Adv. Nano Res.*, **8**(1), 37-47. https://doi.org/10.12989/anr.2020.8.1.037

Garg, A., Chalak, H., Zenkour, A., Belarbi, M.O. and Sahoo, R. (2022), "Bending and free vibration analysis of symmetric and unsymmetric functionally graded CNT reinforced sandwich beams containing softcore", *Thin Wall. Struct.*, **170**, 108626. https://doi.org/10.1016/j.tws.2021.108626

Ghadiri, M., Hosseini, S., Karami, M. and Namvar, M. (2018), "In-plane and out of plane free vibration of U-shaped AFM probes based on the nonlocal elasticity", *J. Solid Mech.*, **10**(2), 285-299.

Ghadiri Rad, M.H., Shahabian, F. and Hosseini, S.M. (2021), "Two-dimensional geometrically nonlinear hyperelastic wave propagation analysis in FG thick hollow cylinders using MLPG method", *AUT J. Civil Eng.*, 5(3), 465-480. https://doi.org/10.22060/ajce.2021.19911.5752

Hamidi, A., Zidour, M., Bouakkaz, K. and Bensattalah, T. (2018), "Thermal and small-scale effects on vibration of embedded armchair single-walled carbon nanotubes", *J. Nano Res.*, **51**, 24-38. https://doi.org/10.4028/www.scientific.net/JNanoR.51.24

Hamidi, B.A., Hosseini, S.A. and Hayati, H. (2020), "Forced torsional vibration of nanobeam via nonlocal strain gradient theory and surface energy effects under moving harmonic torque", *Wave Random Complex Med.*, 1-16. https://doi.org/10.1080/17455030.2020.1772523

Hayati, H., Hosseini, S.A. and Rahmani, O. (2017), "Coupled twist–bending static and dynamic behavior of a curved single-walled carbon nanotube based on nonlocal theory", *Microsyst. Technol.*, **23**(7), 2393-2401. https://doi.org/10.1007/s00542-016-2933-0

Heidari, Y., Arefi, M. and Irani-Rahaghi, M. (2021), "Free vibration analysis of cylindrical micro/nano-shell reinforced with CNTRC patches", *Int. J. Appl. Mech.*, 2150040. https://doi.org/10.1142/S175882512150040X

Hosseini, S. and Rahmani, O. (2016), "Surface effects on buckling of double nanobeam system based on nonlocal Timoshenko model", *Int. J. Struct. Stabil. Dyn.*, **16**(10), 1550077. https://doi.org/10.1142/S0219455415500777

Hosseini, S. and Rahmani, O. (2017), "Exact solution for axial and transverse dynamic response of functionally graded nanobeam under moving constant load based on nonlocal elasticity theory", *Meccanica*, **52**(6), 1441-1457. https://doi.org/10.1007/s11012-016-0491-2

Hosseini, S., Moghaddam, M. and Rahmani, O. (2020), "Exact solution for axial vibration of the power, exponential and sigmoid FG nonlocal nanobeam", *Adv. Aircr. Spacecr. Sci.*, **7**(6), 517-536. https://doi.org/10.12989/aas.2020.7.6.517

Kaiser, J.P., Roesslein, M., Buerki-Thurnherr, T. and Wick, P. (2011), "Carbon nanotubes-curse or blessing", *Curr. Med. Chem.*, **18**(14), 2115-2128. https://doi.org/10.2174/092986711795656171

Khosravi, F. and Hosseini, S.A. (2020), "On the viscoelastic carbon nanotube mass nanosensor using torsional forced vibration and Eringen's nonlocal model", *Mech. Based Des. Struct.*, 1-24. https://doi.org/10.1080/15397734.2020.1744001

Khosravi, F., Hosseini, S.A. and Hamidi, B.A. (2020a), "Torsional Vibration of nanowire with equilateral triangle cross section based on nonlocal strain gradient for various boundary conditions: comparison with hollow elliptical cross section", *Eur. Phys. J. Plus*, **135**(3), 1-20. https://doi.org/10.1140/epjp/s13360-020-00312-z

Khosravi, F., Simyari, M., Hosseini, S. and Ghadiri, M. (2020b), "An analytical solution on size dependent longitudinal dynamic response of SWCNT under axial moving harmonic load", *J. Solid Mech.*, **12**(3), 586-599. https://doi.org/10.22034/jsm.2019.1875642.1476

Madenci, E. (2021), "Free vibration analysis of carbon nanotube RC nanobeams with variational approaches", *Adv. Nano Res.*, **11**(2), 157-171.https://doi.org/10.12989/anr.2021.11.2.157

Mantari, J., Bonilla, E. and Soares, C.G. (2014), "A new tangential-exponential higher order shear deformation theory for advanced composite plates", *Compos. Part B Eng.*, **60**, 319-328. https://doi.org/10.1016/j.compositesb.2013.12.001

Mohammadjani, R. and Shariyat, M. (2020), "Nonlinear thermomechanical vibration mitigation analysis in rotating fractional-order viscoelastic bidirectional FG annular disks under nonuniform shocks", *J. Therm. Stress.*, **43**(7), 829-873. https://doi.org/10.1080/01495739.2020.1748555

Nielsen, L.E. (1974), "The thermal and electrical conductivity of two-phase systems", *Ind. Eng. Chem. Fund.*, **13**(1), 17-20. https://doi.org/10.1021/i160049a004

Serajzadeh, F. and Malekzadeh, P. (2021), "Two-dimensional low-velocity impact analysis of curved sandwich beams with FG-CNTRC face sheets and porous core", *Mech. Based Des. Struct. Mach.*, 1-22. https://doi.org/10.1080/15397734.2021.2013879

Shariyat, M. and Abedi, S. (2022), "An accurate hyper-elasticity-based plate theory and nonlinear energy-based micromechanics for impact and shock analyses of compliant particle-reinforced FG hyperelastic plates", *ZAMM J. Appl. Math. Mech.*, e202100099. https://doi.org/10.1002/zamm.202100099

Shen, H.S. and Xiang, Y. (2013), "Nonlinear analysis of nanotube-reinforced composite beams resting on elastic foundations in thermal environments", *Eng. Struct.*, **56**, 698-708. https://doi.org/10.1016/j.engstruct.2013.06.002

Şimşek, M. and Reddy, J. (2013), "Bending and vibration of functionally graded microbeams using a new higher order beam theory and the modified couple stress theory", *Int. J. Eng. Sci.*, **64**, 37-53. https://doi.org/10.1016/j.ijengsci.2012.12.002

Tayeb, T.S., Zidour, M., Bensattalah, T., Heireche, H., Benahmed, A. and Bedia, E. (2020), "Mechanical buckling of FG-CNTs reinforced composite plate with parabolic distribution using Hamilton's energy principle", *Advances in nano research*. **8**(2), 135-148.https://doi.org/10.12989/anr.2020.8.2.135

Tounsi, A., Benguediab, S., Semmah, A. and Zidour, M. (2013), "Nonlocal effects on thermal buckling properties of double-walled carbon nanotubes", *Adv. Nano Res.*, **1**(1), 1. https://doi.org/10.12989/anr.2013.1.1.001

Van Quyen, N., Van Thanh, N., Quan, T.Q. and Duc, N.D. (2021), "Nonlinear forced vibration of sandwich cylindrical panel with negative Poisson's ratio auxetic honeycombs core and CNTRC face sheets", *Thin Wall. Struct.*, **162**, 107571. https://doi.org/10.1016/j.tws.2021.107571

Wattanasakulpong, N. and Ungbhakorn, V. (2013), "Analytical solutions for bending, buckling and vibration responses of carbon nanotube-reinforced composite beams resting on elastic foundation", *Comput. Mater. Sci.*, **71**, 201-208. https://doi.org/10.1016/j.commatsci.2013.01.028

Xu, J., Yang, Z., Yang, J. and Li, Y. (2021a), "Free vibration analysis of rotating FG-CNT reinforced composite beams in thermal environments with general boundary conditions", *Aerosp. Sci. Technol.*, **118**, 107030. https://doi.org/10.1016/j.ast.2021.107030.

Xu, X., Zhang, C., Khan, A., Sebaey, T.A. and Alkhedher, M. (2021b), "Free vibrations of rotating CNTRC beams in thermal environment", *Case Stud. Therm. Eng.*, **28**, 101355. https://doi.org/10.1016/j.csite.2021.101355

Zerrouki, R., Karas, A. and Zidour, M. (2020), "Critical buckling analyses of nonlinear FG-CNT reinforced nano-composite beam", *Adv. Nano Res.*, **9**(3), 211-220. https://doi.org/10.12989/anr.2020.9.3.211

Zhang, M. and Li, J. (2009), "Carbon nanotube in different shapes", *Mater. Today*, **12**(6), 12-18. https://doi.org/10.1016/S1369-7021(09)70176-2

Zheng, J., Zhang, C., Musharavati, F., Khan, A., Sebaey, T.A. and Eyvazian, A. (2021), "Forced vibration characteristics of embedded graphene oxide powder reinforced metal foam nanocomposite plate in thermal environment", *Case Stud. Therm. Eng.*, 101167. https://doi.org/10.1016/j.csite.2021.101167

AT

Appendix

$$u_1 = 1, u_2 = \frac{-1+I\sqrt{3}}{2}, \qquad u_3 = \frac{-1-I\sqrt{3}}{2}$$

$$\Delta_0 = {g_4}^2 - 3g_6g_2, \Delta_1 = 2{g_4}^3 - 9g_6g_4g_2 + 27{g_6}^2g_0, Ci = \sqrt[3]{\frac{\Delta_1 + \sqrt{{\Delta_1}^2 - 4{\Delta_0}^3}}{2}} \tag{54}$$

$$x_1 = \frac{-1}{3g_6}\left(g_4 + u_1 Ci + \frac{\Delta_0}{u_1 Ci}\right),\ x_2 = \frac{-1}{3g_6}\left(g_4 + u_2 Ci + \frac{\Delta_0}{u_2 Ci}\right),\ x_3 = \frac{-1}{3g_6}\left(g_4 + u_3 Ci + \frac{\Delta_0}{u_3 Ci}\right)$$

$$\begin{aligned}
y_1 &= -d_6d_{12}d_{17} + d_3d_{15}d_{17} + d_7d_{12}d_{17}d_{18} + d_6d_{13}d_{17}d_{18} + d_6d_{14}d_{17}d_{18} - d_4d_{15}d_{17}d_{18} - d_5d_{15}d_{17}d_{18} - d_3d_{16}d_{17}d_{18} - \\
&d_7d_{13}d_{17}d_{18}^2 - d_7d_{14}d_{17}d_{18}^2 + d_4d_{16}d_{17}d_{18}^2 + d_5d_{16}d_{17}d_{18}^2 \\
y_2 &= d_6^2d_8 - 2d_3d_6d_{12} + d_1d_{12}^2 + d_3^2d_{15} - d_1d_8d_{15} - d_2d_6^2d_{18} - 2d_6d_7d_8d_{18} - d_6^2d_9d_{18} - d_6^2d_{10}d_{18} - d_6^2d_{11}d_{18} + \\
&2d_4d_6d_{12}d_{18} + 2d_5d_6d_{12}d_{18} + 2d_3d_7d_{12}d_{18} - d_2d_{12}^2d_{18} + 2d_3d_6d_{13}d_{18} - 2d_1d_{12}d_{13}d_{18} + 2d_3d_6d_{14}d_{18} - 2d_1d_{12}d_{14}d_{18} + \\
&d_1d_2d_{15}d_{18} - 2d_3d_4d_{15}d_{18} - 2d_3d_5d_{15}d_{18} + d_2d_8d_{15}d_{18} + d_1d_9d_{15}d_{18} + d_1d_{10}d_{15}d_{18} + d_1d_{11}d_{15}d_{18} - d_3^2d_{16}d_{18} + \\
&d_1d_8d_{16}d_{18} + 2d_2d_6d_7d_{18}^2 + d_7^2d_8d_{18}^2 + 2d_6d_7d_9d_{18}^2 + 2d_6d_7d_{10}d_{18}^2 + 2d_6d_7d_{11}d_{18}^2 - 2d_4d_7d_{12}d_{18}^2 - 2d_5d_7d_{12}d_{18}^2 - \\
&2d_4d_6d_{13}d_{18}^2 - 2d_5d_6d_{13}d_{18}^2 - 2d_3d_7d_{13}d_{18}^2 + 2d_2d_{12}d_{13}d_{18}^2 + d_1d_{13}^2d_{18}^2 - 2d_4d_6d_{14}d_{18}^2 - 2d_5d_6d_{14}d_{18}^2 - 2d_3d_7d_{14}d_{18}^2 + \\
&2d_2d_{12}d_{14}d_{18}^2 + 2d_1d_{13}d_{14}d_{18}^2 + d_1d_{14}^2d_{18}^2 - d_2^2d_{15}d_{18}^2 + d_4^2d_{15}d_{18}^2 + 2d_4d_5d_{15}d_{18}^2 + d_5^2d_{15}d_{18}^2 - d_2d_9d_{15}d_{18}^2 - d_2d_{10}d_{15}d_{18}^2 - \\
&d_2d_{11}d_{15}d_{18}^2 - d_1d_2d_{16}d_{18}^2 + 2d_3d_4d_{16}d_{18}^2 + 2d_3d_5d_{16}d_{18}^2 - d_2d_8d_{16}d_{18}^2 - d_1d_9d_{16}d_{18}^2 - d_1d_{10}d_{16}d_{18}^2 - d_1d_{11}d_{16}d_{18}^2 - \\
&d_2d_7^2d_{18}^3 - d_7^2d_9d_{18}^3 - d_7^2d_{10}d_{18}^3 - d_7^2d_{11}d_{18}^3 + 2d_4d_7d_{13}d_{18}^3 + 2d_5d_7d_{13}d_{18}^3 - d_2d_{13}^2d_{18}^3 + 2d_4d_7d_{14}d_{18}^3 + 2d_5d_7d_{14}d_{18}^3 - \\
&2d_2d_{13}d_{14}d_{18}^3 - d_2d_{14}^2d_{18}^3 + d_2^2d_{16}d_{18}^3 - d_4^2d_{16}d_{18}^3 - 2d_4d_5d_{16}d_{18}^3 - d_5^2d_{16}d_{18}^3 + d_2d_9d_{16}d_{18}^3 + d_2d_{10}d_{16}d_{18}^3 + d_2d_{11}d_{16}d_{18}^3 \\
y_3 &= -d_6d_{12}d_{19} + d_3d_{15}d_{19} + d_7d_{12}d_{19}d_{20} + d_6d_{13}d_{19}d_{20} + d_6d_{14}d_{19}d_{20} - d_4d_{15}d_{19}d_{20} - d_5d_{15}d_{19}d_{20} - d_3d_{16}d_{19}d_{20} - \\
&d_7d_{13}d_{19}d_{20}^2 - d_7d_{14}d_{19}d_{20}^2 + d_4d_{16}d_{19}d_{20}^2 + d_5d_{16}d_{19}d_{20}^2 \\
y_4 &= d_6^2d_8 - 2d_3d_6d_{12} + d_1d_{12}^2 + d_3^2d_{15} - d_1d_8d_{15} - d_2d_6^2d_{20} - 2d_6d_7d_8d_{20} - d_6^2d_9d_{20} - d_6^2d_{10}d_{20} - d_6^2d_{11}d_{20} + \\
&2d_4d_6d_{12}d_{20} + 2d_5d_6d_{12}d_{20} + 2d_3d_7d_{12}d_{20} - d_2d_{12}^2d_{20} + 2d_3d_6d_{13}d_{20} - 2d_1d_{12}d_{13}d_{20} + 2d_3d_6d_{14}d_{20} - \\
&2d_1d_{12}d_{14}d_{20} + d_1d_2d_{15}d_{20} - 2d_3d_4d_{15}d_{20} - 2d_3d_5d_{15}d_{20} + d_2d_8d_{15}d_{20} + d_1d_9d_{15}d_{20} + d_1d_{10}d_{15}d_{20} + d_1d_{11}d_{15}d_{20} - \\
&d_3^2d_{16}d_{20} + d_1d_8d_{16}d_{20} + 2d_2d_6d_7d_{20}^2 + d_7^2d_8d_{20}^2 + 2d_6d_7d_9d_{20}^2 + 2d_6d_7d_{10}d_{20}^2 + 2d_6d_7d_{11}d_{20}^2 - 2d_4d_7d_{12}d_{20}^2 - \\
&2d_5d_7d_{12}d_{20}^2 - 2d_4d_6d_{13}d_{20}^2 - 2d_5d_6d_{13}d_{20}^2 - 2d_3d_7d_{13}d_{20}^2 + 2d_2d_{12}d_{13}d_{20}^2 + d_1d_{13}^2d_{20}^2 - 2d_4d_6d_{14}d_{20}^2 - \\
&2d_5d_6d_{14}d_{20}^2 - 2d_3d_7d_{14}d_{20}^2 + 2d_2d_{12}d_{14}d_{20}^2 + 2d_1d_{13}d_{14}d_{20}^2 + d_1d_{14}^2d_{20}^2 - d_2^2d_{15}d_{20}^2 + d_4^2d_{15}d_{20}^2 + 2d_4d_5d_{15}d_{20}^2 + \\
&d_5^2d_{15}d_{20}^2 - d_2d_9d_{15}d_{20}^2 - d_2d_{10}d_{15}d_{20}^2 - d_2d_{11}d_{15}d_{20}^2 - d_1d_2d_{16}d_{20}^2 + 2d_3d_4d_{16}d_{20}^2 + 2d_3d_5d_{16}d_{20}^2 - d_2d_8d_{16}d_{20}^2 - \\
&d_1d_9d_{16}d_{20}^2 - d_1d_{10}d_{16}d_{20}^2 - d_1d_{11}d_{16}d_{20}^2 - d_2d_7^2d_{20}^3 - d_7^2d_9d_{20}^3 - d_7^2d_{10}d_{20}^3 - d_7^2d_{11}d_{20}^3 + 2d_4d_7d_{13}d_{20}^3 + 2d_5d_7d_{13}d_{20}^3 - \\
&d_2d_{13}^2d_{20}^3 + 2d_4d_7d_{14}d_{20}^3 + 2d_5d_7d_{14}d_{20}^3 - 2d_2d_{13}d_{14}d_{20}^3 - d_2d_{14}^2d_{20}^3 + d_2^2d_{16}d_{20}^3 - d_4^2d_{16}d_{20}^3 - 2d_4d_5d_{16}d_{20}^3 - \\
&d_5^2d_{16}d_{20}^3 + d_2d_9d_{16}d_{20}^3 + d_2d_{10}d_{16}d_{20}^3 + d_2d_{11}d_{16}d_{20}^3 \\
y_5 &= -d_6d_{12}d_{21} + d_3d_{15}d_{21} + d_7d_{12}d_{21}d_{22} + d_6d_{13}d_{21}d_{22} + d_6d_{14}d_{21}d_{22} - d_4d_{15}d_{21}d_{22} - d_5d_{15}d_{21}d_{22} - \\
&d_3d_{16}d_{21}d_{22} - d_7d_{13}d_{21}d_{22}^2 - d_7d_{14}d_{21}d_{22}^2 + d_4d_{16}d_{21}d_{22}^2 + d_5d_{16}d_{21}d_{22}^2 \\
y_6 &= d_6^2d_8 - 2d_3d_6d_{12} + d_1d_{12}^2 + d_3^2d_{15} - d_1d_8d_{15} - d_2d_6^2d_{22} - 2d_6d_7d_8d_{22} - d_6^2d_9d_{22} - d_6^2d_{10}d_{22} - d_6^2d_{11}d_{22} + \\
&2d_4d_6d_{12}d_{22} + 2d_5d_6d_{12}d_{22} + 2d_3d_7d_{12}d_{22} - d_2d_{12}^2d_{22} + 2d_3d_6d_{13}d_{22} - 2d_1d_{12}d_{13}d_{22} + 2d_3d_6d_{14}d_{22} - \\
&2d_1d_{12}d_{14}d_{22} + d_1d_2d_{15}d_{22} - 2d_3d_4d_{15}d_{22} - 2d_3d_5d_{15}d_{22} + d_2d_8d_{15}d_{22} + d_1d_9d_{15}d_{22} + d_1d_{10}d_{15}d_{22} + d_1d_{11}d_{15}d_{22} - \\
&d_3^2d_{16}d_{22} + d_1d_8d_{16}d_{22} + 2d_2d_6d_7d_{22}^2 + d_7^2d_8d_{22}^2 + 2d_6d_7d_9d_{22}^2 + 2d_6d_7d_{10}d_{22}^2 + 2d_6d_7d_{11}d_{22}^2 - 2d_4d_7d_{12}d_{22}^2 - \\
&2d_5d_7d_{12}d_{22}^2 - 2d_4d_6d_{13}d_{22}^2 - 2d_5d_6d_{13}d_{22}^2 - 2d_3d_7d_{13}d_{22}^2 + 2d_2d_{12}d_{13}d_{22}^2 + d_1d_{13}^2d_{22}^2 - 2d_4d_6d_{14}d_{22}^2 - \\
&2d_5d_6d_{14}d_{22}^2 - 2d_3d_7d_{14}d_{22}^2 + 2d_2d_{12}d_{14}d_{22}^2 + 2d_1d_{13}d_{14}d_{22}^2 + d_1d_{14}^2d_{22}^2 - d_2^2d_{15}d_{22}^2 + d_4^2d_{15}d_{22}^2 + 2d_4d_5d_{15}d_{22}^2 + \\
&d_5^2d_{15}d_{22}^2 - d_2d_9d_{15}d_{22}^2 - d_2d_{10}d_{15}d_{22}^2 - d_2d_{11}d_{15}d_{22}^2 - d_1d_2d_{16}d_{22}^2 + 2d_3d_4d_{16}d_{22}^2 + 2d_3d_5d_{16}d_{22}^2 - d_2d_8d_{16}d_{22}^2 - \\
&d_1d_9d_{16}d_{22}^2 - d_1d_{10}d_{16}d_{22}^2 - d_1d_{11}d_{16}d_{22}^2 - d_2d_7^2d_{22}^3 - d_7^2d_9d_{22}^3 - d_7^2d_{10}d_{22}^3 - d_7^2d_{11}d_{22}^3 + 2d_4d_7d_{13}d_{22}^3 + 2d_5d_7d_{13}d_{22}^3 - \\
&d_2d_{13}^2d_{22}^3 + 2d_4d_7d_{14}d_{22}^3 + 2d_5d_7d_{14}d_{22}^3 - 2d_2d_{13}d_{14}d_{22}^3 - d_2d_{14}^2d_{22}^3 + d_2^2d_{16}d_{22}^3 - d_4^2d_{16}d_{22}^3 - 2d_4d_5d_{16}d_{22}^3 - \\
&d_5^2d_{16}d_{22}^3 + d_2d_9d_{16}d_{22}^3 + d_2d_{10}d_{16}d_{22}^3 + d_2d_{11}d_{16}d_{22}^3
\end{aligned}$$

$$\begin{aligned}
g_0 &= d_6^2d_8 - 2d_3d_6d_{12} + d_1d_{12}^2 + d_3^2d_{15} - d_1d_8d_{15} \\
g_2 &= d_2d_6^2 + 2d_6d_7d_8 + d_6^2d_9 + d_6^2d_{10} + d_6^2d_{11} - 2d_4d_6d_{12} - 2d_5d_6d_{12} - 2d_3d_7d_{12} + d_2d_{12}^2 - 2d_3d_6d_{13} + 2d_1d_{12}d_{13} - \\
&2d_3d_6d_{14} + 2d_1d_{12}d_{14} - d_1d_2d_{15} + 2d_3d_4d_{15} + 2d_3d_5d_{15} - d_2d_8d_{15} - d_1d_9d_{15} - d_1d_{10}d_{15} - d_1d_{11}d_{15} + d_3^2d_{16} - d_1d_8d_{16} \\
g_4 &= 2d_2d_6d_7 + d_7^2d_8 + 2d_6d_7d_9 + 2d_6d_7d_{10} + 2d_6d_7d_{11} - 2d_4d_7d_{12} - 2d_5d_7d_{12} - 2d_4d_6d_{13} - 2d_5d_6d_{13} - \\
&2d_3d_7d_{13} + 2d_2d_{12}d_{13} + d_1d_{13}^2 - 2d_4d_6d_{14} - 2d_5d_6d_{14} - 2d_3d_7d_{14} + 2d_2d_{12}d_{14} + 2d_1d_{13}d_{14} + d_1d_{14}^2 - d_2^2d_{15} + d_4^2d_{15} + \\
&2d_4d_5d_{15} + d_5^2d_{15} - d_2d_9d_{15} - d_2d_{10}d_{15} - d_2d_{11}d_{15} - d_1d_2d_{16} + 2d_3d_4d_{16} + 2d_3d_5d_{16} - d_2d_8d_{16} - d_1d_9d_{16} - d_1d_{10}d_{16} \\
&\qquad - d_1d_{11}d_{16} \\
g_6 &= d_2d_7^2 + d_7^2d_9 + d_7^2d_{10} + d_7^2d_{11} - 2d_4d_7d_{13} - 2d_5d_7d_{13} + d_2d_{13}^2 - 2d_4d_7d_{14} - 2d_5d_7d_{14} + 2d_2d_{13}d_{14} + d_2d_{14}^2 - \\
&d_2^2d_{16} + d_4^2d_{16} + 2d_4d_5d_{16} + d_5^2d_{16} - d_2d_9d_{16} - d_2d_{10}d_{16} - d_2d_{11}d_{16}
\end{aligned} \tag{56}$$

$$\begin{aligned}
f_0 &= \frac{-d_6d_{12}d_{17} + d_3d_{15}d_{17}}{d_{18}} - \frac{r_1y_1}{d_{18}y_2} + \frac{-d_6d_{12}d_{19} + d_3d_{15}d_{19}}{d_{20}} - \frac{r_1y_3}{d_{20}y_4} + \frac{-d_6d_{12}d_{21} + d_3d_{15}d_{21}}{d_{22}} - \frac{r_1y_5}{d_{22}y_6} \\
r_1 &= d_6^2d_8 - 2d_3d_6d_{12} + d_1d_{12}^2 + d_3^2d_{15} - d_1d_8d_{15} \\
f_4 &= -\frac{r_2y_1}{y_2} - \frac{r_2y_3}{y_4} - \frac{r_2y_5}{y_6} \\
r_2 &= d_2d_7^2 + d_7^2d_9 + d_7^2d_{10} + d_7^2d_{11} - 2d_4d_7d_{13} - 2d_5d_7d_{13} + d_2d_{13}^2 - 2d_4d_7d_{14} - 2d_5d_7d_{14} + 2d_2d_{13}d_{14} + d_2d_{14}^2 - \\
&d_2^2d_{16} + d_4^2d_{16} + 2d_4d_5d_{16} + d_5^2d_{16} - d_2d_9d_{16} - d_2d_{10}d_{16} - d_2d_{11}d_{16} \\
f_2 &= -\frac{y_1}{d_{18}^2} - \frac{y_1r_3}{d_{18}^2y_2} - \frac{y_3}{d_{20}^2} - \frac{y_3r_3}{d_{20}^2y_4} - \frac{y_5}{d_{22}^2} - \frac{y_5r_3}{d_{22}^2y_6} \\
r_3 &= -d_6^2d_8 + 2d_3d_6d_{12} - d_1d_{12}^2 - d_3^2d_{15} + d_1d_8d_{15} + d_2d_6^2d_{18} + 2d_6d_7d_8d_{18} + d_6^2d_9d_{18} + d_6^2d_{10}d_{18} + d_6^2d_{11}d_{18} - \\
&2d_4d_6d_{12}d_{18} - 2d_5d_6d_{12}d_{18} - 2d_3d_7d_{12}d_{18} + d_2d_{12}^2d_{18} - 2d_3d_6d_{13}d_{18} + 2d_1d_{12}d_{13}d_{18} - 2d_3d_6d_{14}d_{18} + 2d_1d_{12}d_{14}d_{18} - \\
&d_1d_2d_{15}d_{18} + 2d_3d_4d_{15}d_{18} + 2d_3d_5d_{15}d_{18} - d_2d_8d_{15}d_{18} - d_1d_9d_{15}d_{18} - d_1d_{10}d_{15}d_{18} - d_1d_{11}d_{15}d_{18} + d_3^2d_{16}d_{18} - d_1d_8d_{16}d_{18}
\end{aligned} \tag{57}$$

$$
\begin{aligned}
&y_7 = d_6^2 d_{17} - d_1 d_{15} d_{17} - 2d_6 d_7 d_{17} d_{18} + d_2 d_{15} d_{17} d_{18} + d_1 d_{16} d_{17} d_{18} + d_7^2 d_{17} d_{18}^2 - d_2 d_{16} d_{17} d_{18}^2\\
&y_8 = d_6^2 d_{19} - d_1 d_{15} d_{19} - 2d_6 d_7 d_{19} d_{20} + d_2 d_{15} d_{19} d_{20} + d_1 d_{16} d_{19} d_{20} + d_7^2 d_{19} d_{20}^2 - d_2 d_{16} d_{19} d_{20}^2\\
&y_9 = d_6^2 d_{21} - d_1 d_{15} d_{21} - 2d_6 d_7 d_{21} d_{22} + d_2 d_{15} d_{21} d_{22} + d_1 d_{16} d_{21} d_{22} + d_7^2 d_{21} d_{22}^2 - d_2 d_{16} d_{21} d_{22}^2\\
&J_0 = \frac{d_6^2 d_{17} - d_1 d_{15} d_{17}}{d_{18}} - \frac{r_1 y_7}{d_{18} y_2} + \frac{d_6^2 d_{19} - d_1 d_{15} d_{19}}{d_{20}} - \frac{r_1 y_8}{d_{20} y_4} + \frac{d_6^2 d_{21} - d_1 d_{15} d_{21}}{d_{22}} - \frac{r_1 y_9}{d_{22} y_6}\\
&J_2 = \frac{-d_6^2 d_{17} + d_1 d_{15} d_{17} + 2d_6 d_7 d_{17} d_{18} - d_2 d_{15} d_{17} d_{18} - d_1 d_{16} d_{17} d_{18}}{d_{18}^2} - \frac{r_3 y_7}{d_{18}^2 y_2} +\\
&\frac{-d_6^2 d_{19} + d_1 d_{15} d_{19} + 2d_6 d_7 d_{19} d_{20} - d_2 d_{15} d_{19} d_{20} - d_1 d_{16} d_{19} d_{20}}{d_{20}^2} - \frac{r_4 y_8}{d_{20}^2 y_4} +\\
&\frac{-d_6^2 d_{21} + d_1 d_{15} d_{21} + 2d_6 d_7 d_{21} d_{22} - d_2 d_{15} d_{21} d_{22} - d_1 d_{16} d_{21} d_{22}}{d_{22}^2} - \frac{r_5 y_9}{d_{22}^2 y_6}\\
&r_4 = -d_6^2 d_8 + 2d_3 d_6 d_{12} - d_1 d_{12}^2 - d_3^2 d_{15} + d_1 d_8 d_{15} + d_2 d_6^2 d_{20} + 2d_6 d_7 d_8 d_{20} + d_6^2 d_9 d_{20} + d_6^2 d_{10} d_{20} + d_6^2 d_{11} d_{20} -\\
&2d_4 d_6 d_{12} d_{20} - 2d_5 d_6 d_{12} d_{20} - 2d_3 d_7 d_{12} d_{20} + d_2 d_{12}^2 d_{20} - 2d_3 d_6 d_{13} d_{20} + 2d_1 d_{12} d_{13} d_{20} - 2d_3 d_6 d_{14} d_{20} + 2d_1 d_{12} d_{14} d_{20} -\\
&d_1 d_2 d_{15} d_{20} + 2d_3 d_4 d_{15} d_{20} + 2d_3 d_5 d_{15} d_{20} - d_2 d_8 d_{15} d_{20} - d_1 d_9 d_{15} d_{20} - d_1 d_{10} d_{15} d_{20} - d_1 d_{11} d_{15} d_{20} + d_3^2 d_{16} d_{20} - d_1 d_8 d_{16} d_{20}\\
&r_5 = -d_6^2 d_8 + 2d_3 d_6 d_{12} - d_1 d_{12}^2 - d_3^2 d_{15} + d_1 d_8 d_{15} + d_2 d_6^2 d_{22} + 2d_6 d_7 d_8 d_{22} + d_6^2 d_9 d_{22} + d_6^2 d_{10} d_{22} + d_6^2 d_{11} d_{22} -\\
&2d_4 d_6 d_{12} d_{22} - 2d_5 d_6 d_{12} d_{22} - 2d_3 d_7 d_{12} d_{22} + d_2 d_{12}^2 d_{22} - 2d_3 d_6 d_{13} d_{22} + 2d_1 d_{12} d_{13} d_{22} - 2d_3 d_6 d_{14} d_{22} +\\
&2d_1 d_{12} d_{14} d_{22} - d_1 d_2 d_{15} d_{22} + 2d_3 d_4 d_{15} d_{22} + 2d_3 d_5 d_{15} d_{22} - d_2 d_8 d_{15} d_{22} - d_1 d_9 d_{15} d_{22} - d_1 d_{10} d_{15} d_{22} - d_1 d_{11} d_{15} d_{22} +\\
&d_3^2 d_{16} d_{22} - d_1 d_8 d_{16} d_{22}\\
&J_4 = -\frac{r_2 y_7}{y_2} - \frac{r_2 y_8}{y_4} - \frac{r_2 y_9}{y_6}
\end{aligned}
\tag{58}
$$

$$
\begin{aligned}
&y_{10} = -d_3 d_6 d_{17} + d_1 d_{12} d_{17} + d_4 d_6 d_{17} d_{18} + d_5 d_6 d_{17} d_{18} + d_3 d_7 d_{17} d_{18} - d_2 d_{12} d_{17} d_{18} - d_1 d_{13} d_{17} d_{18} - d_1 d_{14} d_{17} d_{18} -\\
&d_4 d_7 d_{17} d_{18}^2 - d_5 d_7 d_{17} d_{18}^2 + d_2 d_{13} d_{17} d_{18}^2 + d_2 d_{14} d_{17} d_{18}^2\\
&y_{11} = -d_3 d_6 d_{19} + d_1 d_{12} d_{19} + d_4 d_6 d_{19} d_{20} + d_5 d_6 d_{19} d_{20} + d_3 d_7 d_{19} d_{20} - d_2 d_{12} d_{19} d_{20} - d_1 d_{13} d_{19} d_{20} - d_1 d_{14} d_{19} d_{20} -\\
&d_4 d_7 d_{19} d_{20}^2 - d_5 d_7 d_{19} d_{20}^2 + d_2 d_{13} d_{19} d_{20}^2 + d_2 d_{14} d_{19} d_{20}^2\\
&y_{12} = -d_3 d_6 d_{21} + d_1 d_{12} d_{21} + d_4 d_6 d_{21} d_{22} + d_5 d_6 d_{21} d_{22} + d_3 d_7 d_{21} d_{22} - d_2 d_{12} d_{21} d_{22} - d_1 d_{13} d_{21} d_{22} - d_1 d_{14} d_{21} d_{22} -\\
&d_4 d_7 d_{21} d_{22}^2 - d_5 d_7 d_{21} d_{22}^2 + d_2 d_{13} d_{21} d_{22}^2 + d_2 d_{14} d_{21} d_{22}^2
\end{aligned}
\tag{59}
$$

$$
\begin{aligned}
&R_0 = \frac{-d_3 d_6 d_{17} + d_1 d_{12} d_{17}}{d_{18}} - \frac{r_1 y_{10}}{d_{18} y_2} + \frac{-d_3 d_6 d_{19} + d_1 d_{12} d_{19}}{d_{20}} - \frac{r_1 y_{11}}{d_{20} y_4} + \frac{-d_3 d_6 d_{21} + d_1 d_{12} d_{21}}{d_{22}} - \frac{r_1 y_{12}}{d_{22} y_6}\\
&R_2 = \frac{d_3 d_6 d_{17} - d_1 d_{12} d_{17} - d_4 d_6 d_{17} d_{18} - d_5 d_6 d_{17} d_{18} - d_3 d_7 d_{17} d_{18} + d_2 d_{12} d_{17} d_{18} + d_1 d_{13} d_{17} d_{18} + d_1 d_{14} d_{17} d_{18}}{d_{18}^2} - \frac{r_3 y_{10}}{d_{18}^2 y_2} +\\
&\frac{d_3 d_6 d_{19} - d_1 d_{12} d_{19} - d_4 d_6 d_{19} d_{20} - d_5 d_6 d_{19} d_{20} - d_3 d_7 d_{19} d_{20} + d_2 d_{12} d_{19} d_{20} + d_1 d_{13} d_{19} d_{20} + d_1 d_{14} d_{19} d_{20}}{d_{20}^2} - \frac{r_4 y_{11}}{d_{20}^2 y_4} +\\
&\frac{d_3 d_6 d_{21} - d_1 d_{12} d_{21} - d_4 d_6 d_{21} d_{22} - d_5 d_6 d_{21} d_{22} - d_3 d_7 d_{21} d_{22} + d_2 d_{12} d_{21} d_{22} + d_1 d_{13} d_{21} d_{22} + d_1 d_{14} d_{21} d_{22}}{d_{22}^2} - \frac{r_5 y_{12}}{d_{22}^2 y_6}\\
&R_4 = -\frac{r_2 y_{10}}{y_2} - \frac{r_2 y_{11}}{y_4} - \frac{r_2 y_{12}}{y_6}
\end{aligned}
\tag{60}
$$

$$
\begin{aligned}
&d_1 = A_{11}\alpha^2, d_2 = I_0, d_3 = B_{11}\alpha^3 - C_{110}\alpha^3, d_4 = I_1\alpha, d_5 = -I_3\alpha, d_6 = C_{110}\alpha^2,\\
&d_7 = I_3, d_8 = -2E_{11}\alpha^4 + H_{11}\alpha^4 + D_{11}\alpha^4 + A_{55}\alpha^2 + k_w + k_s\alpha^2 - N_{x0}\alpha^2,\\
&d_9 = I_2\alpha^2, d_{10} = -2I_4\alpha^2, d_{11} = I_5\alpha^2, d_{12} = -H_{11}\alpha^3 + E_{11}\alpha^3 - A_{55}\alpha,\\
&d_{13} = I_4\alpha, d_{14} = -I_5\alpha, d_{15} = H_{11}\alpha^2 + A_{55}, d_{16} = I_5, d_{17} = 2P_1V_1\alpha, d_{18} = V_1\alpha,\\
&d_{19} = P_2(V_2\alpha + \omega), d_{20} = (V_2\alpha + \omega)^2, d_{21} = P_2(\omega - V_2\alpha), d_{22} = (\omega - V_2\alpha)^2
\end{aligned}
\tag{61}
$$